Rezaee Sh. et al.
July 2026
Urban Economics and Planning
Volume 7, Issue 4

Spatio-temporal dynamics of LULC and vegetation structure and their relationship with the urban heat island phenomenon in Rasht

Shahriar Rezaee[1], Aliakbar Salaripour[2*]

1. M.Sc. Student in urban planning, Department of Urban Studies, Faculty of Architecture and Art, University of Guilan, Rasht, Iran
2. Associate professor, Department of Urban Design and Planning, Faculty of Architecture and Arts, University of Guilan, Rasht, Iran

Original Article

Received: 2025/10/31
Revised: 2025/11/22
Accepted: 2025/11/23

HOW TO CITE THIS ARTICLE

Rezaee Sh. Salaripour A. Spatio-temporal dynamics of LULC and vegetation structure and their relationship with the urban heat island phenomenon in Rasht. *Urban Economics and Planning* 7(4):20-52.

DOI: 10.22034/uep.2025.556211.1756

Abstract

Rapid and uncontrolled urbanization in the humid megacities of northern Iran, such as Rasht, has transformed agricultural and green lands into impermeable surfaces, intensifying the urban heat island (UHI) effect and reducing the urban quality of life. This study examines the long-term dynamics of land use and land cover (LULC) and their impact on land surface temperature (LST) patterns in Rasht from 2000 to 2024. Thermal data from Landsat satellites were used to extract LST with sensor-specific algorithms. Multi-temporal mosaicking and radiometric normalization were applied to address SLC errors in ETM+. LULC and urban structure maps were generated using Landsat and Sentinel-2 imagery, incorporating spectral indices such as NDVI, NDBI, DBI, and EBBI. The study examined the correlations between land cover/urban structure and surface temperature. Results show that built-up areas increased from 41% to 63%, while green cover and agricultural lands decreased, correlating with a significant rise in LST and the highest average temperature recorded in 2016. A strong negative correlation between NDVI and LST (-0.7 to -0.8) and a high positive correlation between construction indices and LST (0.6 to 0.8) highlight the role of impermeable surfaces and fragmented green buffers in urban warming. The study suggests enhancing green-blue networks (including wetlands and agricultural lands), developing continuous green corridors, and utilizing reflective and permeable materials as key strategies to improve thermal resilience and support climate-responsive urban planning in Rasht.

Keywords

Land surface temperature (LST)
Land use diversity
Land use/land cover (LULC) change
Spatio-temporal analysis
Surface urban heat island (SUHI)
Thermal infrared remote sensing

* Corresponding Author: salaripour@guilan.ac.ir

1. Introduction

The urban heat island (UHI) phenomenon is one of the most significant environmental and climatic challenges faced by cities today, directly affecting quality of life, energy consumption, and public health (Sharmin & Chappell, 2025; Wei, Lemoy, & Caruso, 2024; Siswanto et al., 2023; Ramsay et al., 2023). This phenomenon refers to higher temperatures in urban areas compared to surrounding rural or suburban regions. The main factors contributing to the formation and intensification of UHI are land use change (LUC) and land use/land cover (LULC) transformation as a result of urban expansion. The conversion of natural surfaces, such as vegetation, into artificial ones, like asphalt, concrete, and buildings, leads to a decrease in albedo (surface reflectivity) and evapotranspiration, while increasing solar energy absorption. As a result, these processes lead to an increase in land surface temperature (LST) and ambient air temperature (Gazi et al., 2021; Koko et al., 2021; Sharma & Vashishtha, 2023). The consequences of this phenomenon on public health and energy are significant: exposure to heat increases health risks and the demand for cooling, while changes in atmospheric chemical composition and pollution dynamics can further degrade air quality (Li et al., 2019; wang et al., 2024).

1.1. Role of LULC and vegetation cover

One of the primary drivers of SUHI is LULC changes, which increase impermeable surfaces at the expense of urban green cover. The removal of trees and green spaces reduces the cooling capacity through decreased evapotranspiration and shading, whereas the expansion of asphalt and concrete increases heat storage during the day and its release at night (Tang et al., 2017; Zafar et al., 2024). Recent research confirms the role of ecological land and green infrastructure in mitigating urban heat stress when their extent and spatial continuity are maintained or enhanced (Tan et al., 2021; Feng et al., 2021). Human-induced heat emissions from buildings and cooling systems can exacerbate thermal effects by adding direct heat to the urban boundary layer (Alhazmi et al., 2022). Meanwhile, traffic and industrial activities also impact thermal patterns and air quality (Wang et al., 2024). Together, these processes intensify urban warming and amplify UHI signals in many growing cities (Wei et al., 2024).

1.2. Specific characteristics of Rasht and the need for study

In this broad context, the city of Rasht, a major metropolis in northern Iran, has experienced rapid spatial expansion, population growth, and intense construction activity over recent decades. These developments have led to significant changes in the LULC pattern and urban vegetation cover, which may have a meaningful impact on SUHI dynamics. In humid cities like Rasht, where a mosaic of diverse vegetation covers, natural irrigation networks, and traditional agricultural systems (such as rice paddies and tea gardens) are integrated into the urban fabric, the interaction between moisture levels and surface features can modulate the intensity and spatial distribution of UHI (Sharmin & Chappell, 2025; Zafar et al., 2024). Understanding the relationship between LULC heterogeneity, vegetation cover arrangements, and LST patterns in such environments is essential for managing heat risks, improving outdoor thermal comfort, reducing cooling energy load, and achieving synergies in air quality improvement (Li et al., 2019; Wang et al., 2024).

1.3. Research aim, scope, and approach

The primary objective of this study is to comprehensively analyze the relationships between land use and land cover changes, vegetation structure, and the intensity of urban surface heat islands (SUHI) in the city of Rasht and its surrounding areas. To this end, the present study adopts a multi-step approach, first mapping land use diversity and vegetation structure within the urban and suburban regions of Rasht, and then assessing the differences in land surface temperature (LST) across various combinations of land use and vegetation cover. Subsequently, the spatial intensity pattern and distribution of thermal hotspots within urban areas are analyzed to identify critical heat zones. Finally, through spatial statistical modeling, the links between LULC heterogeneity, vegetation structure, and SUHI intensity are elucidated. The results provide a scientific foundation for developing urban planning strategies that focus on enhancing green infrastructure, improving the spatial continuity of natural areas, and smart land use management to reduce thermal stress and increase the climate resilience of Rasht. For the long-term period from 2000 to 2024, LULC and LST data were

extracted from Landsat/Sentinel satellite imagery, atmospheric and radiometric corrections were applied, and temporal alignment was ensured. Multiple indices, such as NDVI, NDBI, DBI, and EBBI, were used to examine the relationship between SUHI and landscape composition and configuration, considering related variables (solar radiation, cloud cover, wind, material properties, and urban density) (Tang et al., 2017; Li et al., 2019; Alhazmi et al., 2022).

1.4. Global background and importance of vegetation configuration

Numerous remote sensing studies confirm that land use and land cover (LULC) changes are a primary factor in intensifying urban surface heat islands (SUHIs), and this dependence remains stable across different spatial and temporal scales. A study in Guangzhou, using the predictive scale, showed that rapid urbanization is likely to disrupt the balance of cooling covers by 2032, with water bodies such as rivers and wetlands decreasing by 46.97%, vegetation cover decreasing by 34.24%, and built-up areas experiencing a dramatic increase of 263.71%. As a result, the ratio of high and moderately high-temperature areas will increase by 127.76% and 375.92%, respectively, indicating a significant intensification of SUHI (Xiang et al., 2024). Similarly, in Changchun, urban areas increased more than fourfold between 1984 and 2014, and the proportion of UHI areas rose from 15.27% to 29.62%. The average LST in urban areas was always higher than that in rural surroundings and showed a strong positive correlation with the proportion of impermeable surfaces (Yang et al., 2017). In the Phoenix metropolitan area, the conversion of land to residential and impermeable uses significantly amplified both the daytime and nighttime SUHI signals. At the same time, vegetation covers effectively reduced LST through increased evapotranspiration and heat storage mitigation (wang et al., 2016). Similarly, in Delhi and Mumbai, ongoing warming, the formation of thermal hotspots, and a reduction in the urban thermal comfort index (UTFVI) have been observed, confirming the sensitivity of SUHI to LULC indices, particularly NDVI (Shahfahad et al., 2022). However, it is not solely the amount of vegetation that determines a city's thermal response; instead, spatial configuration and landscape coherence also play a critical role. In Changchun, the increase in vegetation cover and NDVI was correlated with a significant reduction in LST (r = -0.62 to -0.81), while fragmentation and patch complexity increased surface temperature through higher indices (PD, LSI, Split). In contrast, the spatial connectivity and coherence of vegetation cover, as indicated by increased metrics (AI, Cohesion, LP), have demonstrated significant cooling effects. With only a 10% increase in the aggregation index, resulting in a reduction in LST of approximately 1.9 to 3.8 °C. This effect is amplified at larger spatial scales. Such findings are particularly relevant for humid cities with mosaic green-blue landscapes, such as Rasht, as they emphasize the simultaneous importance of both the extent and configuration of vegetation in modulating SUHI intensity and restoring the surface energy balance (Zhibin et al., 2015). At a smaller scale, results from UHI mapping at the street level using urban IoT sensor networks show that high-density built-up environments, due to the higher thermal capacity of construction materials, exhibit less daily temperature fluctuation and remain warmer at night. In contrast, the continuity and extent of urban green spaces enhance the sustainability of "cool" spots. Evidence shows that the nighttime cooling effect of parks extends beyond the adjacent river areas. The magnitude of this effect depends on vegetation characteristics, urban morphology, and the sky view factor (Jang et al., 2024). Methodologically, two significant advancements in recent SUHI research have emerged. First, the use of machine learning algorithms to predict LST and identify morphological heat drivers. Among these methods, deep neural networks (DNN) and extreme gradient boosting (XGB) models demonstrated higher predictive accuracy in a study on Shiraz. Though temporal dynamics and land use change (LUCC) scenarios were only partially considered (Tanoori et al., 2024). The second advancement involves the development of spatial-temporal hybrid approaches for generating high-resolution continuous LST maps (30 meters), combining random forest (RF) downscaling models with the FSDF model. This combined approach enables more accurate SUHI monitoring, showing that summer SUHI intensity in Chengdu increased from 2.78 °C to 4.04 °C between 2009 and 2018, with the most significant warming observed in impermeable surfaces and the least in water bodies (Yao et al., 2020).

1.5. Analytical insights from previous studies in the context of this research

Despite these methodological advancements, significant research gaps remain. Many studies have overlooked socio-economic drivers and climate change scenarios, and have not provided sufficient process

explanations for key physical mechanisms such as albedo changes, thermal inertia, and surface moisture availability (Xiang et al., 2024; Tanoori et al., 2024). The framework of the present research directly addresses these deficiencies by combining support vector machine (SVM) classification, the mono-window algorithm for retrieving land surface temperature (LST), and cellular automata-artificial neural network (CA-ANN) modeling to predict urban and thermal dynamics up to 2032. In this framework, multi-source indices, including NDVI, NDBI, DBI, and EBBI, along with auxiliary variables (solar radiation, cloud cover, wind, material properties, and urban density), are jointly analyzed to reveal the spatial heterogeneity of LULC and its linkages with urban thermal behavior. Complementary advancements in deep learning and RGB-based remote sensing analysis have shown that neural network architectures can significantly improve the accuracy of urban base map extraction. Although these methods are not directly focused on UHI, they demonstrate the potential for integrating AI and remote sensing to enhance LULC classification and predict urban thermal variability (Benayad et al., 2025). Furthermore, recent climatic studies have confirmed that climate change and land-use transformation synergistically alter the thermal structure of landscapes. Increased temperatures and changes in precipitation patterns lead to reduced vegetation cover, altered surface hydrology, and disruption of the energy-moisture balance at the surface, resulting in the emergence of localized thermal anomalies and increased LST. This conceptual synergy highlights the necessity for an integrated LULC-climate framework to investigate SUHI dynamics in humid urban environments, such as Rasht, where ecological heterogeneity and human-induced pressures coexist simultaneously (Karimi et al., 2025).

2. Materials and methods

The study area is the city of Rasht, the capital of Guilan province in northern Iran. To examine the spatial-temporal dynamics of land use and land cover (LULC) and their relationship with the intensity of urban heat islands (UHI), multi-temporal satellite imagery was applied. The data used include imagery from Landsat satellites (OLI, ETM+, OLI) and Sentinel-2, covering four representative summer periods: 2000, 2008, 2016, and 2024, obtained from the USGS Earth Explorer database. For 2008, Landsat 7 (ETM+) data were used, while for subsequent years, Landsat 8 data were utilized. The summer season was specifically chosen because, during other seasons, extensive cloud cover in Rasht limits access to high-quality imagery. All images underwent standard radiometric, atmospheric, and geometric corrections prior to analysis to ensure uniformity and comparability of the data across different time periods. For atmospheric corrections, the QUAC (Quick Atmospheric Correction) algorithm was used, which effectively corrects atmospheric effects and enhances the accuracy of satellite data for remote sensing analysis. This algorithm is particularly suitable for Landsat and Sentinel-2 data, accurately correcting atmospheric effects such as light scattering and pollutants. The preprocessing process was carried out in Envi 5.3 software following established multi-temporal remote sensing analysis protocols. Regarding the use of Landsat and Sentinel-2 data, it is worth noting that these two sensors, with differing spatial and temporal resolutions, are combined for various purposes. Sentinel-2 was used to improve LULC classification (with higher spatial resolution and more spectral bands), while Landsat was employed to extract LST (using more accurate thermal data). This combination enabled more precise results and effectively mitigated the limitations of each sensor. Supervised classification using the maximum likelihood classifier (MLC) algorithm was employed to generate land use maps for each year. The main land use classes included built-up areas, vegetation cover, agricultural land, and water bodies. Classification accuracy was evaluated using high-resolution imagery from Google Earth. These images were used for comparing and assessing the accuracy of the classification results. Land surface temperature (LST) was extracted using the mono-window algorithm with thermal bands from Landsat TM band 6. For Landsat 8 (TIRS) and Sentinel-2, which lack thermal bands, the generalized single-channel method (GSCM) algorithm was used to extract LST from Landsat 8 data, with NDVI as an auxiliary index for Sentinel-2. Subsequently, LST maps were integrated with the normalized difference vegetation index (NDVI) and LULC data to identify urban heat island areas. Minimum, maximum, and average LST values for five administrative districts in Rasht were calculated to accurately map intra-urban thermal variability. The relationship between LULC, vegetation indices, and LST was analyzed using Pearson's correlation coefficient and linear regression. These models quantified the strength and direction of the relationships between UHI intensity and explanatory variables. Therefore, in this study, geographically weighted regression (GWR) was used to investigate the relationship between land surface temperature (LST) and various geographic/spatial variables,

including NDVI, NDBI, EBBI, and DBI. This local modeling approach, which is one of the advanced techniques for spatial data analysis, is particularly suitable for geographic data with strong spatial correlation features. GWR enables the analysis of local correlations where independent variables have varying effects at different spatial locations. Spatial analysis based on GIS was conducted using ArcGIS software to evaluate and compare spatial patterns across the four study periods. By integrating LULC maps, vegetation indices, and LST data, this research provides a comprehensive assessment of how urban expansion and vegetation dynamics affect UHI intensity in Rasht. Consequently, the multi-temporal remote sensing framework and RS–GIS analyses employed in this study are specifically designed to track the spatial and temporal dynamics of land use and land cover, and to explain their relationship with urban heat island intensity in Rasht. Furthermore, the findings of this research can be applied in urban planning, environmental management, and climate change adaptation strategies to help reduce heat-related risks and enhance the thermal resilience of expanding cities.

2.1 Extraction of land surface temperature (LST)

To calculate land surface temperature, the Mono-Window algorithm was used based on the thermal band outputs from Landsat. This process involves three main steps: first, calculating the top-of-atmosphere (TOA) radiance; then, calculating the TOA radiance from the calibration coefficients available in the Landsat metadata and the DN pixel values; and finally, calculating the brightness temperature using the thermal calibration coefficients (K1-K2). Surface emissivity (ε) was extracted from the NDVI model and vegetation cover fraction. The land surface temperature was then calculated as follows:

Radiance (TOA):

$$L\lambda = ML \times Qcal + AL \text{ (Landsat-8/9)}$$

$$L\lambda = ((Lmax - Lmin)/ (Qmax - Qmin)) \times (Qcal - Qmin) + Lmin \text{ (Landsat-5/7)}$$

Brightness Temperature:

$$TB(K) = K2 / Ln (K1 / L\lambda + 1)$$

NDVI-based Emissivity:

$$Pv = ((NDVI - NDVImin) / (NDVImax - NDVImin)) ^2$$

$$\varepsilon = 0.004 \times Pv + 0.986$$

Land Surface Temperature (emissivity-corrected):

$$LST(°C) = TB / (1 + (\Lambda \times TB / 1.438\times10^{-2}) \times \ln \varepsilon) - 273.15$$

To calculate land surface temperature (LST), the effective wavelength (λ) differs across various sensors. For Landsat-8 (band 10), it is approximately 10.895 micrometers (μm), while for Landsat-5/7 (band 6), it is approximately 11.45 micrometers (μm). The calibration constants k1 and k2, as well as the reflectance coefficients (ML and AL) and the values of Lmin/Lmax and Qmin/Qmax, must be directly extracted from the metadata (MTL) file associated with each scene, as these parameters are specific to the image itself and are necessary for accurate calculations of radiative temperature and conversion to surface temperature. In these calculations, the thermal band wavelength and standard coefficients were applied according to USGS guidelines for Landsat sensors. All processes were implemented in ENVI 5.3 and ArcGIS software. Furthermore, the formula for calculating NDVI is as follows:

$$NDVI = (\rho\_NIR - \rho\_RED) / (\rho\_NIR + \rho\_RED)$$

In this equation, (ρ) represents the surface reflectance in each band. This index has values ranging from +1 to -1. Values close to +1 indicate dense and healthy vegetation cover, while values close to -1 represent areas devoid of vegetation, such as urban surfaces, barren land, or water bodies. The mathematical formula for this index (EBBI) is defined as follows:

$$EBBI= (SWIR - NIR) / (10 \times \sqrt{TIR} + NIR)$$

Band mapping (concise):

Landsat-5/7: NIR=b4, SWIR=B5, TIR=B6; Landsat-8/9: NIR=B5, SWIR=B6, TIR=B10

The mathematical formula for this index (DBI) is defined as follows:

$$DBI=(\rho\_Blue - \rho\_TIR) / (\rho\_Blue + \rho\_TIR) - (\rho\_NIR - \rho\_Red) / (\rho\_NIR + \rho\_Red)$$

The normalized difference built-up index (NDBI) is one of the most commonly used spectral indices for identifying and distinguishing urban impervious surfaces. This index takes advantage of the higher reflectance of the short-wave infrared (SWIR) band compared to the near-infrared (NIR) band in built-up materials. It is calculated using the following formula:

$$NDBI = (SWIR - NIR) / (SWIR + NIR)$$

2.2. Study area

The study area, Rasht, the capital of Guilan province in northern Iran, is located in the Guilan plain near the Caspian Sea, with geographic coordinates of 37°16’ N and 49°36’ E. The city is situated at an elevation between 7 and 10 meters above sea level (Figure 1).

The study area corresponds to the administrative boundary of Rasht, which has been extracted using the official polygon layer (marz_Rasht) in ArcGIS, and its estimated area is approximately 101.6 square kilometers. Over the past decades, Rasht has experienced rapid urban growth, with its population increasing from around 600,000 in 1990 to over 1 million in 2024. Rasht has a humid subtropical climate, with annual precipitation ranging from 1,000 to 1,500 millimeters per year. Summers are hot and humid, while winters are mild and rainy. Historically, the predominant landscape of Rasht consisted of rice paddies and the vegetation of the Caspian Hyrcanian forests. However, due to urban expansion, large areas of agricultural land and green spaces have been converted into built-up areas. This transformation of land use and land cover has significantly impacted the land surface temperature (LST) and the dynamics of the urban heat island (UHI). For this research, satellite images from the summer seasons of 2000, 2008, 2016, and 2024 were used to analyze these dynamics. The choice of summer is deliberate, as during other seasons, persistent cloud cover and frequent rainfall significantly reduce the quality and reliability of the images. In contrast, summer images generally exhibit more stable weather conditions and clearer skies, providing a more accurate and reliable basis for analyzing land-use changes, vegetation cover structure, and UHI intensity.

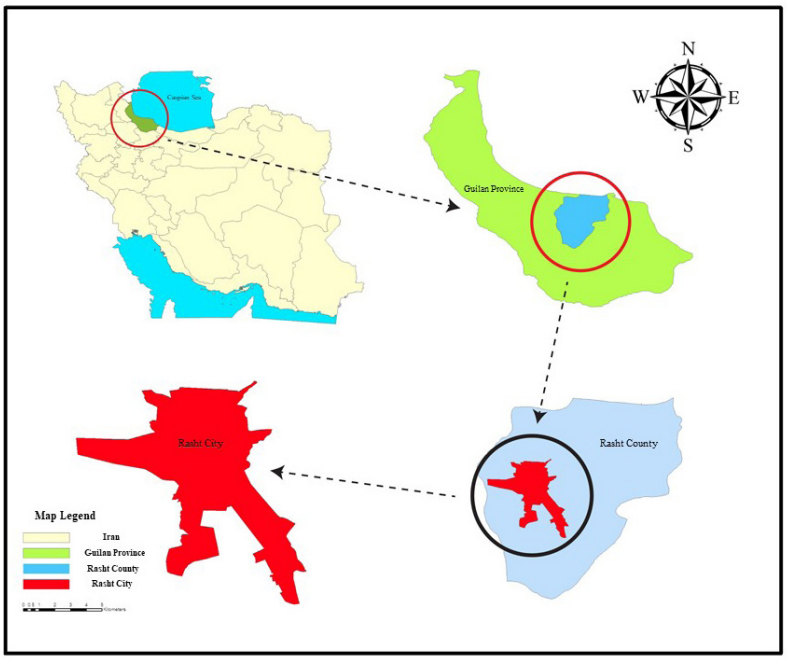

Figure 1. Location of the study area. The city of Rasht (in red) is situated within Rasht county (in blue) and Guilan province (in green), located in northern Iran.

3. Findings

Land use and land cover (LULC) analysis

To extract land use and land cover (LULC) maps, supervised classification was performed on Landsat (OLI-TM) and Sentinel-2 satellite images. In ENVI software version 5.3, training samples were defined as regions of interest (ROI) for four main classes: a) Built-up areas: this includes dense and semi-dense urban fabric, road networks, industrial spaces, and other impervious surfaces (built-up). b) Agricultural and horticultural land: this includes rice paddies, tea and fruit orchards, and other agricultural lands managed under specific planting-harvesting patterns and irrigation regimes (AGRI) .c) Natural vegetation and urban green spaces: This includes riparian green zones, parks, and public green spaces within the city, distinguished from agricultural lands in terms of canopy structure, density, spatial continuity, and ecological function (vegetation). D) Barren land: this includes areas with negligible vegetation cover (less than about 10% density), such as bare soil and degraded lands(bareland). Supervised classification of the images in Envi was conducted using the maximum likelihood classifier (MLC) algorithm, and LULC maps were produced for each of the years 2000, 2008, 2016, and 2024. The dataset included multispectral, cloud-

free images from the summer season, which are particularly suitable for analyzing urban land use changes. The LULC maps for the key years 2000, 2008, 2016, and 2024 have been produced and are presented below. These maps serve as the basis for analyzing spatial and temporal changes in land use, highlighting that transformations in LULC structure are key factors in the formation and intensification of the urban heat island (UHI). As such, these maps, shown in Figure 2, are fundamental for investigating the relationship between land use changes and land surface temperature (LST).

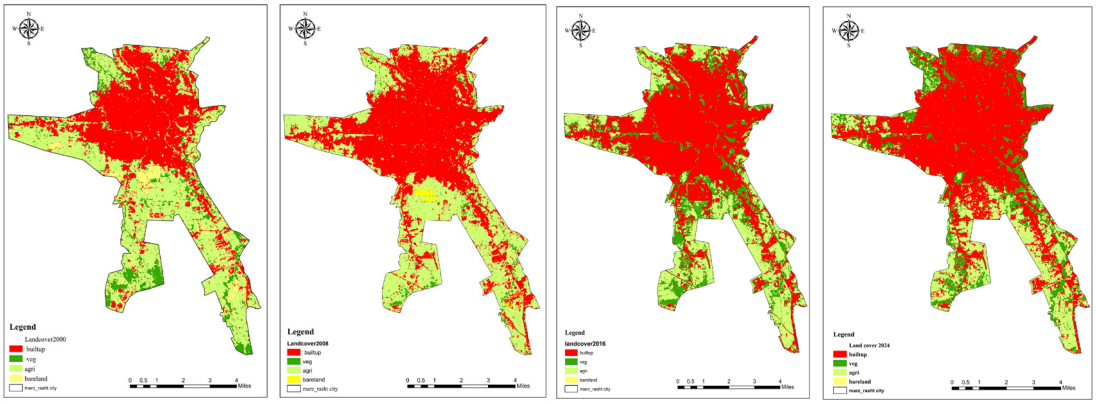

Figure 2. Land use and land cover (LULC) maps for the years 2000, 2008, 2016, and 2024.

Table 1. Area (in square kilometers) and percentage share (%) of land use and land cover classes, including built-up areas, vegetation, agricultural and horticultural lands, and barren land for the years 2000, 2008, 2016, and 2024

Land use classes	2000 (km²)	2000 (%)	2008 (km²)	2008 (%)	2016 (km²)	2016 (%)	2024 (km²)	2024 (%)
Built-up areas	41.28	40.64	55.80	54.92	56.79	55.90	63.48	62.69
Vegetation cover	46.89	46.17	41.77	41.11	27.64	27.20	21.71	21.37
Agricultural and horticultural lands	9.54	9.39	2.78	2.73	17.01	16.74	15.41	15.17
Barren land	3.85	3.79	1.25	1.22	0.14	0.14	0.77	0.75

As shown in Table 1, the built-up areas in Rasht city have continued to expand between 2000 and 2024. The area of this class increased from approximately 41.3 km² (40.64%) in 2000 to 55.8 km² (54.92%) in 2008, and further to 56.8 km² (55.90%) in 2016, ultimately reaching around 63.5 km² (62.69%) in 2024. In contrast, vegetation cover (including Hyrcanian forests and natural/urban green spaces) has experienced a decreasing trend, dropping from around 46.9 km² (46.17%) in 2000 to 41.8 km² (41.11%) in 2008, 27.6 km² (27.20%) in 2016, and 21.7 km² (21.37%) in 2024. Over the entire period, the share of this class has decreased by nearly 25 percentage points. Agricultural and horticultural lands have shown more fluctuating behavior compared to the previous two classes, decreasing from about 9.5 km² (9.39%) in 2000 to 2.8 km² (2.73%) in 2008, but increasing to about 17.0 km² (16.74%) in 2016, before slightly decreasing to 15.4 km² (15.17%) in 2024. Barren land also occupies a relatively small share of the city's area, with a decreasing trend overall throughout the study period. It decreased from approximately 3.9 km² (3.79%) in 2000 to 1.2 km² (1.22%) in 2008 and 0.14 km² (0.14%) in 2016, before slightly increasing to 0.77 km² (0.75%) in 2024. This numerical pattern suggests that the continuous expansion of built-up areas has primarily been accompanied by a steady decline in vegetation cover and a redistribution of agricultural and barren lands, which has contributed to the intensification of the city's thermal response and the enhancement of the urban surface heat island (UHI). Table 2 presents the changes in the area of main land use/land cover classes in Rasht city during the time intervals of 2000–2008, 2008–2016, and 2016–2024, as well as the total change from 2000 to 2024 (areas in square kilometers). In total, the area of built-up areas increased from approximately 41.3 to 63.5 km², with a net increase of about 22.2 km². This growth mainly

occurred during the 2000–2008 (+14.51 km²) and 2016–2024 (+6.79 km²) periods. In contrast, vegetation cover decreased by approximately 25.2 km² over the entire period, with the most significant decline occurring between 2008 and 2016 (-14.1 km²). Agricultural and horticultural lands, after an initial reduction during the 2000–2008 period (-6.8 km²), expanded by approximately 14.2 km² between 2008 and 2016, ultimately resulting in a net increase of 5.9 km² compared to 2000. Barren lands, despite fluctuations between periods, show an overall decrease of about 2.8 km², with a significant increase during 2000–2008 being nearly neutralized by the 2008–2016 period.

Table 2. Changes in area (in square kilometers) and relative changes (%) of land use/land cover classes in Rasht city during the study periods

Land use classes	Built-up areas	Vegetation cover	Agricultural and horticultural lands	Barren land
2000–2008 (km²) δ	+14.51	-5.12	-6.76	-2.60
2000–2008 (%) δ	+14.28	-5.06	-6.66	-2.57
2008–2016 (km²) δ	+1.00	-14.13	+14.24	+1.10
2008–2016 (%) δ	+0.98	-13.91	+14.01	+1.08
2016–2024 (km²) δ	+6.69	-5.93	-1.60	+0.62
2016–2024 (%) δ	+6.79	-5.83	-1.57	+0.62
2000–2024 (km²) δ	+22.20	-25.18	+5.88	+1.97
2000–2024 (%) δ	+22.05	-24.80	+5.78	+1.95

Land surface temperature (LST) analysis

During the four years studied in Rasht city (2000, 2008, 2016, and 2024), the average land surface temperature (LST) has shown noticeable fluctuations. Specifically, the average LST decreased from 31.18°C in 2000 to 27.13°C in 2008, then increased to 32.59°C in 2016, and reached 29.65°C in 2024. The thermal range (minimum-maximum) also follows a similar pattern, decreasing from 23.25–44.83°C in 2000 to 21.50–38.00°C in 2008, then increasing to 25.53–43.69°C in 2016, and stabilizing between 23.11–40.61°C in 2024 (Table 3). These fluctuations in average LST do not necessarily reflect a straightforward trend of urban development, as studies suggest that LST is sensitive not only to land use/land cover (LULC) changes but also to the climatic conditions at the time of image acquisition (air temperature, relative humidity, cloud cover, and solar angle). Therefore, the decrease in average LST in 2008 and 2024 compared to 2000 and 2016 should be attributed to a combination of LULC changes and interannual climatic variations, rather than solely a decrease in urbanization intensity. Additionally, Figure 3 presents the spatial pattern of LST for the years 2000, 2008, 2016, and 2024. In all four years, high LST values (yellow to red colors) are mainly concentrated in the central and parts of the northern and eastern parts of the city, while lower LST values (green colors) are primarily observed in the city's outskirts, particularly in the southern and western areas and some parts of the east. Comparing the maps shows that the extent and continuity of hot spots in 2016 were the largest, covering a broader area in the central, northern, and eastern parts of the city. In 2008, compared to 2000, the areas with very high temperatures were more limited, and a greater portion of the city fell within the moderate temperature ranges. In 2024, while the warm core persisted in the center and east, some of these hot spots shifted to moderate temperature classes compared to 2016, and areas with lower LST remained visible in the city's periphery. Comparing this pattern with the land use/land cover map (Figure 2) reveals that areas with lower LST mostly overlap with agricultural lands and vegetation patches in the southern, western, and part of the eastern outskirts of the city.

In comparison, areas with higher LST correspond to built-up areas and dense urban fabric. This spatial overlap highlights the persistent thermal contrast between the densely built urban core and the greener periphery throughout the study period. It is consistent with the statistical values in Table 2, showing fluctuations in the average and range of LST.at the same time, the quantitative changes in LULC in Table 1 show that the share of built-up areas increased from 40.64% in 2000 to 62.69% in 2024 (a 22.05 percentage point increase), while natural vegetation decreased from 46.17% to 21.37%. The combined share of vegetation and agricultural/horticultural lands

dropped from 55.56% to 36.54%. Between 2016 and 2024, the area of built-up areas increased by 668.86 km², while agricultural and horticultural lands decreased by 159.87 km² and vegetation cover by 592.83 km². These changes, alongside the spatial patterns of LST, suggest that although the average LST is influenced by interannual climatic variations, the location and concentration of hotspots throughout the study period correlate with the expansion of impervious surfaces and the reduction of urban green cover.

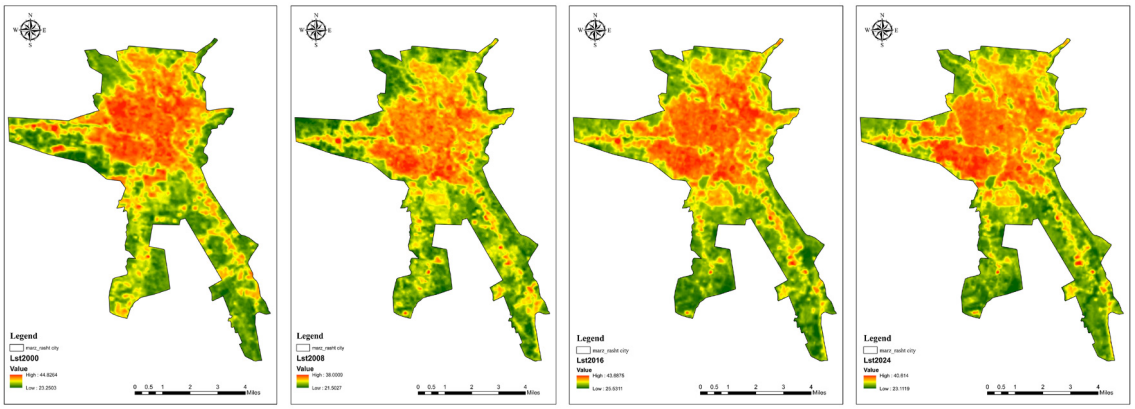

Figure 3. Land surface temperature (LST) maps for the years 2000, 2008, 2016, and 2024

Table 3. Summary statistics of land surface temperature (°c) for the years 2000, 2008, 2016, and 2024

Year	Min LST (°c)	Max LST (°c)	Average LST (°c)	Standard deviation
2000	23.25	44.83	31.18	3.99
2008	21.50	38.00	27.13	2.70
2016	25.53	43.69	32.59	3.40
2024	23.11	40.61	29.65	2.93

Distribution of the normalized difference vegetation index (NDVI) in the study area

The normalized difference vegetation index (NDVI) is one of the most commonly used indicators for measuring the extent and vitality of green vegetation cover. This index is based on the spectral characteristics of healthy plants, utilizing high reflectance in the near-infrared (NIR) band and strong absorption in the red (R) band of the visible spectrum. NDVI values typically range from -1 to +1, where values closer to +1 indicate dense, healthy vegetation, and values closer to -1 represent barren or non-vegetated areas such as urban surfaces, barren land, or water bodies. NDVI is widely used to assess vegetation health, monitor land cover changes, and analyze the spatial distribution of vegetation in a given area.

Normalized difference vegetation index (NDVI) distribution in the study area

The normalized difference vegetation index (NDVI) is one of the most widely used indicators for measuring the extent and vitality of green vegetation cover. This index is based on the spectral characteristics of healthy plants, utilizing high reflectance in the near-infrared (NIR) band and strong absorption in the red (R) band of the visible spectrum.

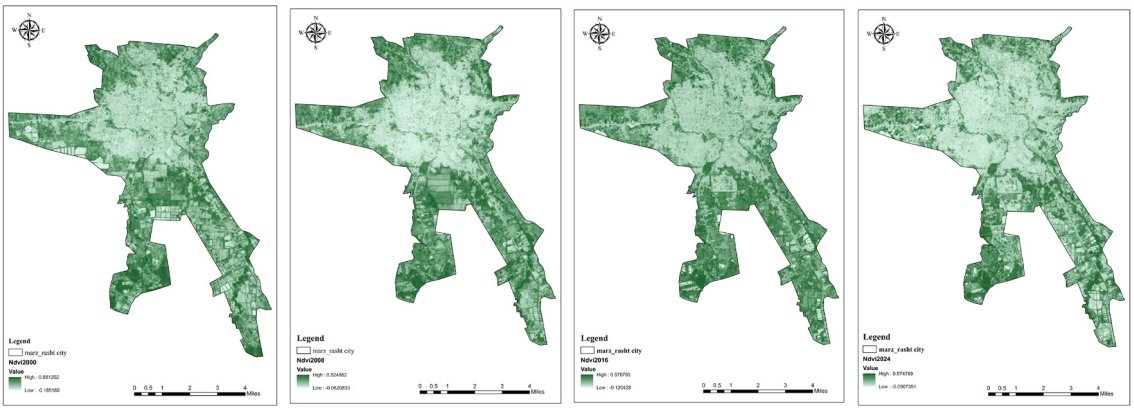

Figure 4. Normalized difference vegetation index (NDVI) maps for Rasht city in the years 2000, 2008, 2016, and 2024

As shown in Figure 4, the pattern of vegetation cover in Rasht city has continuously indicated a reduction in green cover intensity in the dense central-northern urban core over the four study periods. In contrast, peripheral areas, especially in the south and west, have maintained relatively higher NDVI values, with scattered green strips also observed in the east. Between 2000 and 2008, the color spectrum on the maps visibly lightens across the city, with pixels showing medium to high NDVI values decreasing in built-up areas, and signs of fragmentation in urban green spaces becoming apparent. In 2016, a relative recovery was observed, with patches of medium NDVI reappearing along the city outskirts, particularly along drainage paths and irrigation corridors. However, the urban core remains pale, indicating a continued lack of vegetation in the city center. By 2024, the network of green patches will appear more fragmented and smaller than ever before. While the peripheral areas still have higher NDVI values compared to the center, high NDVI cells have retreated toward the outskirts, dividing into small and isolated patches, indicating the process of urban infill and densification. These dynamics observed from the maps align with the land use changes (increase in built-up areas to about 63% by 2024 and a decrease in vegetation and agricultural/ horticultural classes) and the registered land surface temperature (LST) patterns. In 2008, the reduction in NDVI coincided with a period when LST fields showed the best spatial uniformity and the lowest temperature values across the city. The relative recovery of green cover in 2016, despite itself, was overshadowed by the increase in impervious surfaces and was concurrent with the peaks and continuity of thermal patches. In 2024, the NDVI pattern with medium values is mainly found in the city's peripheral areas, with a fragmented and patchy distribution. This distribution corresponds with relatively high surface temperatures and continued development along the east-southeast axis, where impervious surfaces have expanded. Overall, the map results indicate that over the last two decades, Rasht's spatial pattern has evolved from a continuous and cohesive green belt around the periphery to a more fragmented and patchy green matrix surrounding a centrally vegetated, impoverished core. This pattern explains the presence of cooler cells over irrigated and agricultural lands, as well as the repeated thermal patches along the dense central-northern core and the east-southeast extension of the city.

Enhanced built-up and bare soil index (EBBI) distribution in the study area

The enhanced built-up and bare soil index (EBBI) is a single-band index used to differentiate between built-up areas and bare soils simultaneously. It is calculated using the near-infrared (NIR), short-wave infrared (SWIR), and thermal infrared (TIR) bands. This index benefits from higher reflectance in the SWIR band and higher emissivity or brightness temperature of impervious materials compared to the distinct spectral signature of bare soils. By combining spectral reflectance contrasts and thermal surface information, the EBBI enhances the accuracy of differentiating impervious surfaces and bare soils, particularly in dry and semi-arid environments, while reducing confusion with vegetation and water bodies. Since the thermal component (TIR) is included in the definition of EBBI, part of the land surface temperature (LST) information is inherently embedded within this index. Therefore, in this study, the central role of the EBBI is considered as a spatial differentiator for built-up areas and bare soils, and it was excluded as an independent variable in the multivariate regression models for LST.

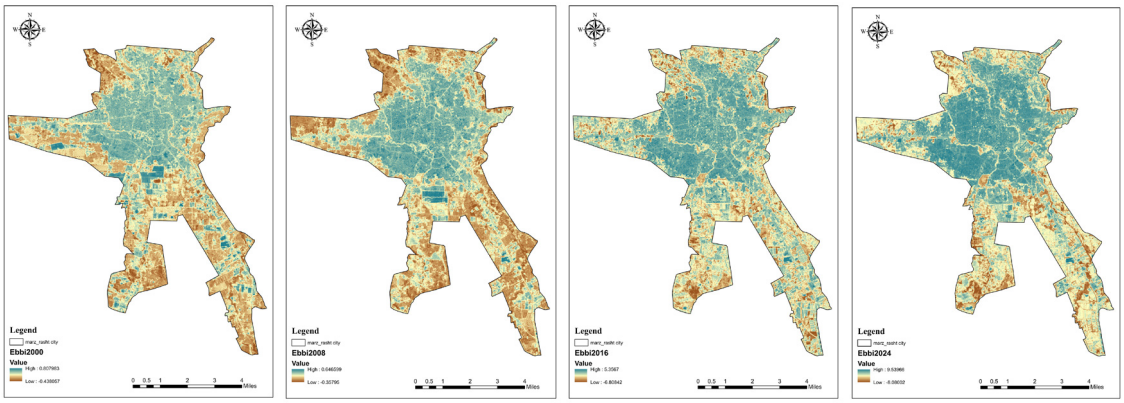

Figure 5. EBBI (enhanced built-up and bare soil index) maps for Rasht city in the years 2000, 2008, 2016, and 2024

Enhanced built-up and bare soil index (EBBI) distribution in the study area

As shown in Figure 5, the enhanced built-up and bare soil index (EBBI), derived from the combination of the near-infrared (NIR), short-wave infrared (SWIR), and thermal infrared (TIR) bands using Landsat thermal data, provides a single-band tool for differentiating urban impervious surfaces and bare soil areas. Higher EBBI values typically indicate areas with built-up or bare soil, while lower values correspond to areas with vegetation or water bodies. In Rasht city, the spatial-temporal pattern of the EBBI indicates a persistent high EBBI core in the central-northern part of the city, with a directional spread of these areas along the east-southeast axis. The highest continuity of high EBBI patches is observed in 2016, and by 2024, although the central cores persist, parts of the former agricultural belt in the north and west of the city have joined the high EBBI areas. These changes align with the land use/land cover (LULC) transformation pattern, where the share of built-up areas increases over the study period, while the areas of vegetation and agricultural/horticultural lands decrease. Comparing the EBBI maps with the land surface temperature (LST) pattern reveals that areas with high EBBI values are predominantly co-located with hotter zones in the urban core and the east-southeast axis. In contrast, areas with lower EBBI values correspond to cooler green belts. However, since the EBBI definition itself includes a thermal component (TIR), the spatial overlap and numerical correlation between EBBI and LST are partly due to the shared thermal information between the two variables. Therefore, this relationship is interpreted as a spectral-spatial match rather than an independent causal relationship. Overall, the increasing continuity and directional expansion of high EBBI areas highlight the replacement of green and agricultural lands with built-up areas and bare soil, whereas medium EBBI patches (with mixed land uses) maintain a more stable role in the city's spatial structure.

Dry built-up index (DBI) distribution in the study area

The dry built-up index (DBI) is a spectral index designed to differentiate between built-up areas and dry or non-vegetated lands, initially proposed for dry and semi-arid environments, where the spectral similarity between dry soils and impervious surfaces reduces the accuracy of conventional indices, such as the NDBI. In the current study, DBI is not employed as an indicator of "climatic dryness," but rather as a tool to locally differentiate between built-up surfaces and bare soils during the summer season. The interpretation of its values is performed relatively, in conjunction with the land use/land cover (LULC) map and high-resolution Google Earth images, reducing the climatic limitations inherent to the original definition of the index. The DBI index enhances the contrast between sparsely vegetated areas (which are often built-up) and bare soils by combining information from the visible, near-infrared (NIR), and thermal infrared (TIR) bands. As a result, it reduces the spectral ambiguity between these two surface types. In this study, DBI was calculated using Landsat-5 and Landsat-8 satellite images for the years 2000, 2008, 2016, and 2024, and its spatial patterns were analyzed alongside NDVI, NDBI, and EBBI indices to interpret the dynamics of impervious surfaces and bare lands at the urban scale. The results indicate that, at the urban scale, DBI effectively highlights areas with limited vegetation cover and thermal patterns corresponding to impervious surfaces. It also reveals the process of converting dry urban lands into built-up areas (due to

infill and urban densification), which aligns with the observed land use changes during the study period (as seen in Figure 4).

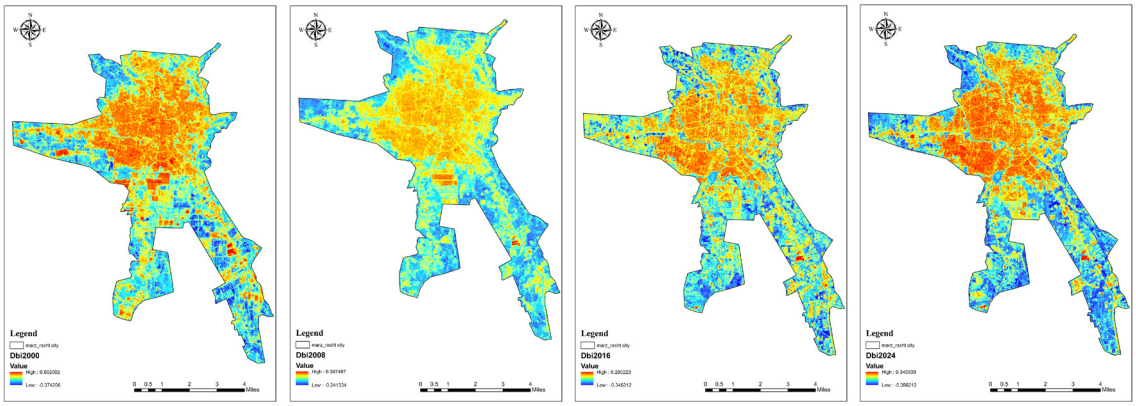

Figure 6. DBI (dry built-up index) maps for Rasht city in the years 2000, 2008, 2016, and 2024

As shown in Figure 6, the spatial pattern of the dry built-up index (DBI) in Rasht city reveals the evolution of urban development and the expansion of impervious surfaces. In 2000, the city's spatial structure was primarily characterized by a single, dense central core with high DBI values in the city center and lower values in the surrounding areas. By 2008, this central core had begun to expand along the development axes aligned with the main access routes, and high DBI patches appeared in the west/southwest and northwest directions around the city, indicating the early signs of a built-up belt forming around the central core. In 2016, these high DBI patches expanded and became more interconnected, with the previously fragmented distribution forming a semi-continuous pattern in the form of a peripheral ring. This pattern is consistent with the process of urban infill within the existing boundaries and edge expansion along the city's periphery. By 2024, the middle ring had become denser and wider, significantly reducing the low-density gaps within the city. Simultaneously, new clusters of high DBI values formed in the outskirts, especially in the west-southwest and northwest directions, pushing the city structure towards a more multi-nodal form. In contrast, the eastern and northeastern areas exhibit a more mixed pattern with weaker continuity. In contrast, in the southern sections, high DBI values increase more linearly and axially. In the central core, DBI values have remained high from the outset, with changes primarily manifesting as increased spatial continuity and infill of interstitial spaces, rather than widespread surface expansion. This transformation aligns with the conversion of agricultural and open lands in the periphery to residential and service uses, as well as the integration and renewal of plots within the designated urban boundary, as shown in the LULC map. Meanwhile, the persistence of lower DBI values in some peripheral areas reflects the continued urban-rural interface. Overall, the DBI spatial patterns indicate the increasing continuity of the built-up fabric, the formation of a dense central ring, and the directional spread of impervious surfaces, which, along with the LST maps, align with the strengthening of the urban heat island in later periods of the study.

Normalized difference built-up index (NDBI) distribution in the study area

The normalized difference built-up index (NDBI) is one of the most widely used spectral indices for identifying and differentiating urban impervious surfaces. Positive values of this index typically represent built-up areas or low-coverage surfaces similar to soil, while negative values correspond to areas with vegetation or water bodies. In this study, the NDBI was extracted using Landsat-5 TM and Landsat-8 OLI satellite images for the years 2000, 2008, 2016, and 2024. At the urban scale, this index clearly distinguishes the boundary between the dense urban core of Rasht and the surrounding agricultural and wetland belts, displaying the increasing expansion of impervious surfaces over time. Particularly in the 2024 scene, the distribution of NDBI values shows a longer positive tail (with a maximum of about 0.37 compared to 0.28 in 2016), and the patches with high NDBI have become more contiguous, especially in the central core, east, and parts of the north of the city. In contrast, the southern areas and much of the western regions still exhibit lower or negative values, corresponding with

agricultural and wetland areas. Given that NDBI may misclassify bright, open soils as urban surfaces, the interpretation in this study was conducted in conjunction with vegetation and land-use layers. The spatial patterns resulting from this analysis are presented in Figure 7.

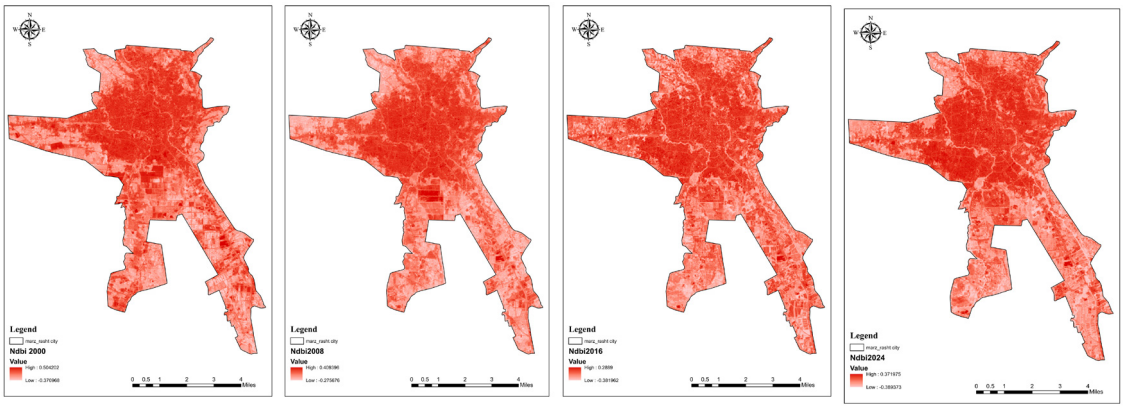

Figure 7. Spatial-temporal distribution of the NDBI (normalized difference built-up index) in Rasht city for the years 2000, 2008, 2016, and 2024

In this study, the NDBI (normalized difference built-up index), defined by the equation (SWIR−NIR)/(SWIR+NIR) (SWIR-NIR) / (SWIR + NIR) (SWIR−NIR)/(SWIR+NIR), was calculated from Landsat TM and OLI satellite images for the years 2000, 2008, 2016, and 2024. To account for radiometric variations between scenes and the effects of seasonal differences in image acquisition times, the resulting maps are presented as continuous gradient spectra. Therefore, Table 3 serves merely as an empirical guide for interpreting and reading the maps.

Table 4. Experimental interpretation key for NDBI in Rasht city: dominant NDBI ranges based on land use classes with diagnostic descriptions, extracted from Landsat TM/OLI satellite data for the period 2000 to 2024

Land use class	Dominant NDBI range	Description
Dense residential area	+0.22 to +0.37	Widespread presence of concrete rooftops, continuous asphalt surfaces, and narrow streets with heavy traffic; indicative of high construction density, severe surface impermeability, and minimal vegetation in the central and highly trafficked urban areas.
Commercial/ industrial	+0.18 to +0.37	Includes warehouses, parking lots, and extensive asphalted or paved areas; these zones have high reflectance in the swir band and typically overlap spatially with dense residential areas. Extremely high impermeability and minimal vegetation are characteristic features of this class.
Suburban / mixed-use	+0.05 to +0.22	A mix of low-density urban areas, open spaces, and scattered green patches, including single-family homes, gardens, and semi-asphalted pathways. These areas generally have medium NDBI values and serve as a transition between dense built-up areas and agricultural or natural vegetation.
Bare dry bright soil	0.00 to +0.18	High reflectance in the SWIR band and slight positive NDBI values; in some cases, it may be confused with built-up surfaces. These lands are typically devoid of vegetation and have very low moisture, found in barren areas or developing urban areas.
Agricultural lands (rice fields/ orchards)	−0.38 to 0.00	Low or near-zero values due to higher reflectance in NIR compared to SWIR during plant growth stages; during irrigation seasons, values may become more negative. These areas typically include wet rice paddies, orchards, and seasonal crops, showing significant spectral fluctuations in multi-temporal imagery.

Land use class	Dominant NDBI range	Description
Urban green spaces/parks	−0.38 to −0.10	Includes permeable vegetation covers such as grass, trees, and shrubs; characterized by high reflectance in NIR and significant absorption in SWIR, resulting in negative NDBI values. These areas play an essential role in urban thermal regulation and lowering land surface temperature (LST), typically found in parks, street edges, and open green spaces.
Open water bodies/wetlands	≤ −0.20	Strongly negative NDBI values due to very low reflectance in SWIR and minimal reflectance in NIR. These areas include wetlands, rivers, ponds, and water-saturated lands, which are typically associated with the lowest land surface temperatures (LSTs) in satellite imagery.

The comparison of the four maps presented in figure 7 demonstrates that the spatial pattern of Rasht city has transformed from a dense, monocentric structure in 2000, with a transparent radial gradient from the center to the periphery and low or negative NDBI values in the peripheral areas (associated with rice paddies, orchards, and wetland belts, including the margins of the Anzali wetland in the west of Rasht), to a structure with a dense central ring and peripheral sub-centers by 2024. In 2008, lateral expansion around the city, particularly to the south and east, became apparent. High to moderate NDBI patches along access routes and ring road paths have increased. Although there is a slight decrease in the maximum local value of the index (which could be due to radiometric, seasonal, or shading differences), the central core has gained more internal continuity. At the same time, the northwest and northeast areas remain at medium to low risk levels. By 2016, the upper tail of the index had been reinforced, and the maximum positive value had reached approximately 0.28. High NDBI patches expanded and connected, transforming the pattern from local dispersion to a semi-continuous peripheral ring. At this stage, low-density gaps within the city have decreased, and medium-density cores have emerged in the central belt. The intensity of the index increased in the east and parts of the north, while the south and parts of the west still had low or negative values, corresponding to agricultural areas and wetland belts. By 2024, the upper threshold of the index had increased from approximately 0.28 to 0.37. The compression in the central core has intensified, the middle ring has gained more continuity, and low-density gaps within the city have been minimized. Sub-centers with high NDBI in the east and north have been consolidated and strengthened, while the south and parts of the west still show low or negative values. Overall, the evidence suggests that the continuity of impervious surfaces has increased, spatial fragmentation has decreased, and the urban pattern has shifted from a monocentric structure to a circular pattern with a tendency toward multiculturalization. This path aligns with development driven by transport infrastructure expansion and the continuation of the urban–agricultural interface, likely indicating the spread and intensification of the urban heat island (UHI) phenomenon in the later study periods.

Distribution of the urban heat island (UHI) phenomenon in the study area

The urban heat island (UHI) phenomenon refers to the condition in which urban areas experience higher temperatures compared to surrounding rural or natural areas. Within the context of surface UHI, this effect is measured by comparing the land surface temperature (LST) within the urban area with the temperature of reference rural or forested areas. The intensity of the urban heat island (UHI) is typically defined as the temperature difference between urban areas and reference areas, expressed by the following equation:

$$UHII = T(urban) - T(rural)$$

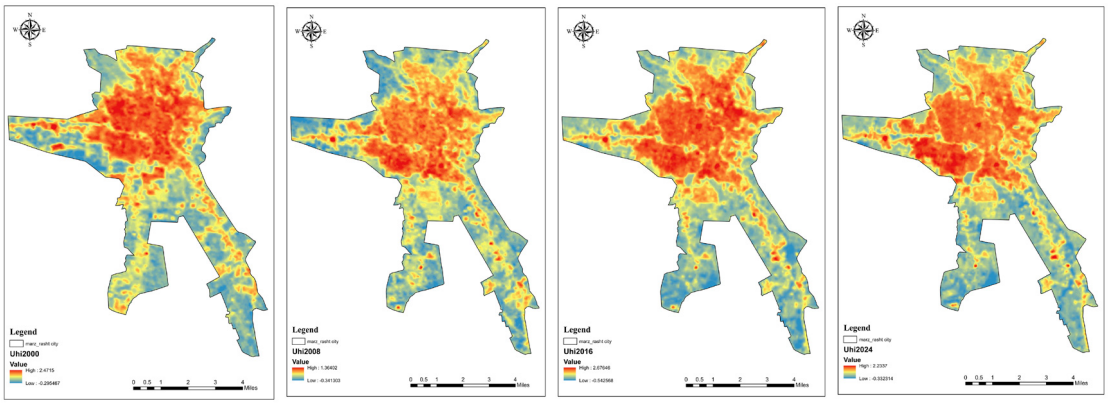

Figure 8. Spatial-temporal changes in urban heat island (UHI) intensity in Rasht city for the years 2000, 2008, 2016, and 2024

The analysis of the four temporal UHI maps in Figure 8 reveals that the thermal pattern of Rasht city has transformed from a "hot core with high intensity and cooler peripheries" at the beginning of the study period to a more moderate thermal concentration in recent years. In 2000, the UHI intensity in the central and eastern parts of the city reached approximately 2.47. The relatively high mean (0.72) and significant standard deviation (0.51) indicate severe thermal heterogeneity and a stark contrast between the dense urban core and the cooler belts in the southern and western areas. These areas, characterized by rice paddies, orchards, and proximity to the Sefidrood River, exhibited negative values around -0.30. This pattern aligns with the spatial morphology of the city's historic section (narrow streets, high aspect ratio, and limited sky view factor [SVF]), where dark impervious surfaces like asphalt and concrete exacerbate the effect. Climatically, Rasht's high humidity, through evapotranspiration in the peripheral areas, helped with cooling, while poor ventilation in the central core hindered heat dissipation. In 2008, the city's thermal field became cooler and more uniform. The maximum intensity decreased to 1.36, with the mean reducing to 0.24 and the standard deviation to 0.28, indicating reduced thermal fluctuations. The cooler zones in the west and northwest (-0.34 °C) persisted, and the scale of the central thermal patch decreased. This moderation was consistent with the stability of surrounding green belts, higher soil moisture, and decreased continuity of impervious surfaces. In 2016, a return of urban heat was observed; the maximum intensity rose to about 2.67, with the mean increasing to 1.00 and the standard deviation rising to 0.70. The thermal patches expanded from the central core towards the north and east, while the southern and western belts (-0.54) continued to function as the city's thermal lungs. Land use changes, including greater density in residential-commercial areas and clusters of industrial zones, increased thermal continuity. At the same time, local climatic regulators (such as mild northern winds and seasonal rainfall) were unable to counterbalance the heat. By 2024, a relative moderation in heat intensity was observed; the maximum value dropped to approximately 2.23, with the mean reducing to 0.55 and the standard deviation to 0.60. The thermal concentration in the central core increased once again, but the southern and western areas remained the coolest parts of the city (around -0.33 to -0.50). This situation aligns with the implementation of targeted green interventions and the use of higher albedo materials in urban renewal projects. However, the continuing high density along principal transport axes still poses a risk of regenerating thermal patches. Overall, the interaction between human and environmental factors suggests that the city's structural layout (high aspect ratio, limited sky view factor, and continuity of impervious surfaces), in conjunction with land cover (wetlands and surrounding green belts), plays a significant role in shaping the UHI patterns in Rasht. Therefore, despite recent moderation, reducing the thermal burden in the core and northeastern parts should be prioritized in urban policies, while preserving and enhancing the southern and western green belts, as vital cooling infrastructure, is essential for the city's future.

Analysis of temporal and spatial trends of urban heat island (UHI) dynamics in Rasht

Table 5. Spatial-temporal dynamics of urban heat island (UHI) indices in Rasht city for the years 2000, 2008, 2016, and 2024

Index	2000	2008	2016	2024	Change range (2000-2008)	Change range (2008-2016)	Change range (2000-2016)	Change range (2016-2024)
Minimum UHI intensity	-0.30	-0.34	-0.54	-0.33	13%	59%	80%	Relative warming in 2024
Maximum UHI intensity	2.47	1.36	2.67	2.23	45%	96%+	8%	Significant decrease by 45% in 2000–2008, thermal return from 2008–2016, then 17% decrease by 2024 due to green policies
Average UHI intensity	0.72	0.24	1.00	0.55	67%	317%+	39%	Sharp decrease by 67% until 2008, significant increase by 317% until 2016, then 23% decrease by 2024, indicating more balanced urban management
Standard deviation	0.51	0.28	0.70	0.60	45% (thermal homogenization)	150%+ (thermal fluctuation increase)	37% (evidence of unbalanced urban expansion)	Thermal homogenization until 2008 (45%), sharp thermal fluctuations in 2016 (150%), and a moderate decrease by 2024
Critical thermal zones	Center - east	Center - north	Center - north-east	Center	Reduced intensity in the eastern part of the city	Increased thermal pressure in the northern and eastern areas	Continued thermal concentration in the central and northern parts	Preserving and maintaining cooling green belts in agricultural and rural zones (rice paddies, tea gardens, wetlands)
Key factors of change	Rapid urban development	Conservation policies	Population growth and construction	Green policies and controlled development	Green projects and regulatory limitations	Weakened regulations and dominance of development-driven approaches	A combination of positive and negative factors	Interaction of urban densification, policy changes, and land use transformation

Correlation of land surface temperature (LST) with NDVI, NDBI, DBI, and EBBI indices using geographically weighted regression (GWR) in the period 2000–2024

This section of the paper focuses on analyzing changes in land surface temperature (LST) and its correlation with various indices, including NDVI, NDBI, DBI, and EBBI, over the time period from 2000 to 2024. The analysis is conducted using geographically weighted regression (GWR), which is particularly suitable for this type of analysis due to its ability to account for spatial correlations and geographical variations in the data. The GWR model allows us to understand the impact of each of these indices on LST at different geographical points over time. In this study, the years 2000 and 2024 are chosen as the start and end points for the changes being analyzed. These years are selected due to significant changes in climatic, urban, and environmental factors both globally and, particularly, in Iran and Rasht city. Using data from these two years allows for an analysis of the 24-year period, which helps to understand the effects of urban development, climate changes, and other factors influencing LST more clearly. The results of these analyses indicate that changes in LST, both locally and over time, have been influenced by various geographical and environmental variables. The findings reveal changes in the mean, minimum, and maximum LST across different periods, and they also examine the relationship between these changes and various environmental indices.

Statistical description of LST variables for 2024

This section provides a statistical description of the land surface temperature (LST) variable. The analysis includes the calculation of key statistical values for the LST data from the year 2024. These values include the mean, minimum, maximum, and standard deviation,

which are used to assess spatial and temporal changes in LST across Rasht city. This information is vital for understanding how temperature varies over time and space and helps in evaluating the accuracy of regression models, particularly GWR, in predicting LST in different regions of the city. The statistical analysis will provide insights into the distribution and fluctuations in LST in the city, offering helpful information for a better understanding of the impacts of urbanization, environmental factors, and climatic variations on temperature patterns in Rasht.

Table 6. Statistical description of the land surface temperature (LST) variable for the year 2024

Index	Value
Observed LST - mean	29.64°c
Observed LST - min	23.21°c
Observed LST - max	38.28°c
Predicted LST - mean	29.70°c
Predicted LST - min	24.58°c
Predicted LST - max	34.96°c
Residual - mean	-0.056°c
Residual - max	+4.70°c
Residual - min	-4.70°c
StdResidual - mean	-0.046°c
StdResidual - max	+6.20°c
StdResidual - min	-4.87°c

Comparison of observed (real LST) and predicted (predicted LST) land surface temperature (LST) with the GWR model

Figure 9 illustrates the comparison between the observed LST (horizontal axis) and the predicted LST (vertical axis) generated by the geographically weighted regression (GWR) model. Most of the data points are clustered around the 45-degree line, indicating a positive correlation and good model performance. The closer the points are to this line, the more accurate the model's LST predictions. The slight scatter of points below the line suggests that predictions are less accurate in certain areas, which may require further investigation to improve model accuracy. This comparison highlights the effectiveness of the GWR model in predicting LST and points to areas where model refinement could be beneficial.

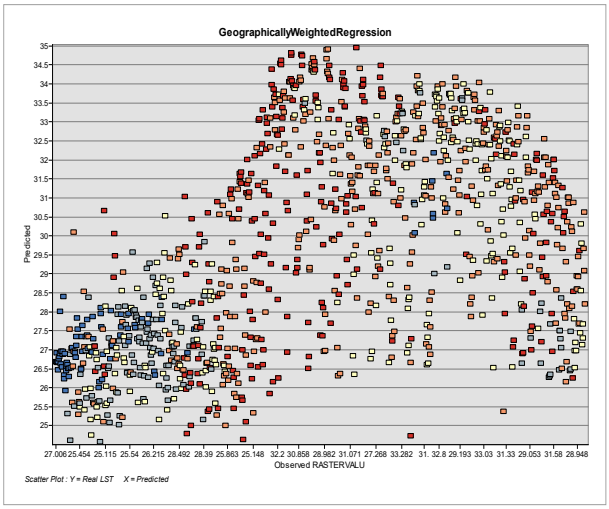

Figure 9. Scatter plot comparing real LST and predicted LST from the GWR model

This boxplot illustrates the distribution of residuals (errors) from the GWR model. It serves as an essential tool for evaluating the accuracy of the model's LST predictions, offering valuable insights into the quality of these predictions. A) interquartile range (IQR): most of the data points fall within the residual range of (--0.6 to 0.6), indicating that the model generally performed well, with prediction errors being limited and acceptable for the majority of the data points. B) outliers: points located outside the box (above or below the whiskers) represent outliers. These points indicate areas where the model has struggled to make accurate predictions, showing significant errors. These regions may exhibit unique land-use changes or unusual environmental characteristics, making predictions particularly challenging. c) Stars and markers: Points marked with stars or asterisks (*) represent extreme outliers, where the model's predictions were particularly inaccurate. These regions warrant further investigation to identify potential factors affecting model accuracy in these areas.

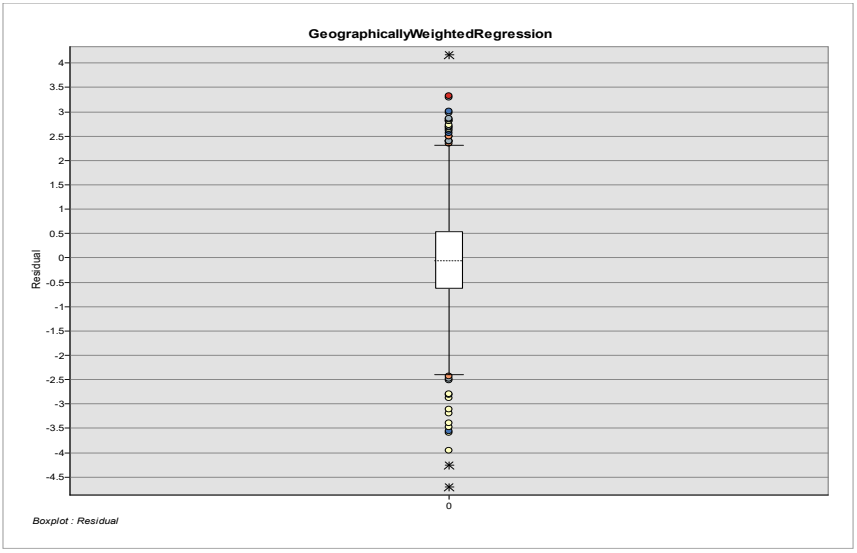

Figure 10. Boxplot of residuals from the geographically weighted regression (GWR) model

Evaluation of the geographically weighted regression (GWR) model quality for analyzing the relationship between LST and environmental indices

This section examines the results of the geographically weighted regression (GWR) model for local R^2. Local R^2 is a metric that indicates how well the model explains the relationship between land surface temperature (LST) and environmental indices, such as NDVI, NDBI, DBI, and EBBI, at a local scale (across different regions of the city). Local R^2 values are specifically used in spatial analysis to identify areas where the model performs well and where improvements are needed. In this study, local R^2 values were calculated for different regions of Rasht city in 2024. The table presented shows that most of the city's areas have local R^2 values ranging from 0.47 to 0.73, indicating good to excellent model performance in these regions. High local R^2 values suggest that the GWR model successfully established a significant relationship between LST and environmental indices, predicting LST with high accuracy. In other words, the model has effectively considered local features such as vegetation (NDVI) and construction density (NDBI) in these areas. However, in some areas of the city, local R^2 values approach zero, indicating that the model lacks high accuracy in these regions. These areas may have lower accuracy for various reasons, such as complex land use changes, outlier data, or the influence of external variables not accounted for in the model. These areas may include regions with rapid land use changes or industrial zones where environmental characteristics differ significantly from the general urban pattern.

Table 7. Distribution of local R^2 values for the geographically weighted regression (GWR) model in analyzing the relationship between land surface temperature (LST) and environmental indices for the year 2024

Index	Value
Mean local R^2	0.576
Minimum local R^2	0.0003
Maximum local R^2	0.916
IQR Local R^2	0.728 - 0.468

In Figure 11, the distribution of local R^2 values is shown based on the frequency of occurrence for each value within different ranges. From this graph, it can be observed that the distribution of local R^2 across most areas of the city forms a multi-peak pattern, indicating varying model performance in different regions. The median local R^2 is approximately 0.576, indicating that the majority of LST predictions have moderate accuracy. The minimum local R^2 value of 0.0003 represents areas where the model had low prediction accuracy. On the other hand, the maximum local R^2 of 0.916 indicates that the model performed exceptionally well in predicting LST in these regions. Overall, the chart shows an approximately symmetric distribution, with a significant portion of the data falling within the medium range.

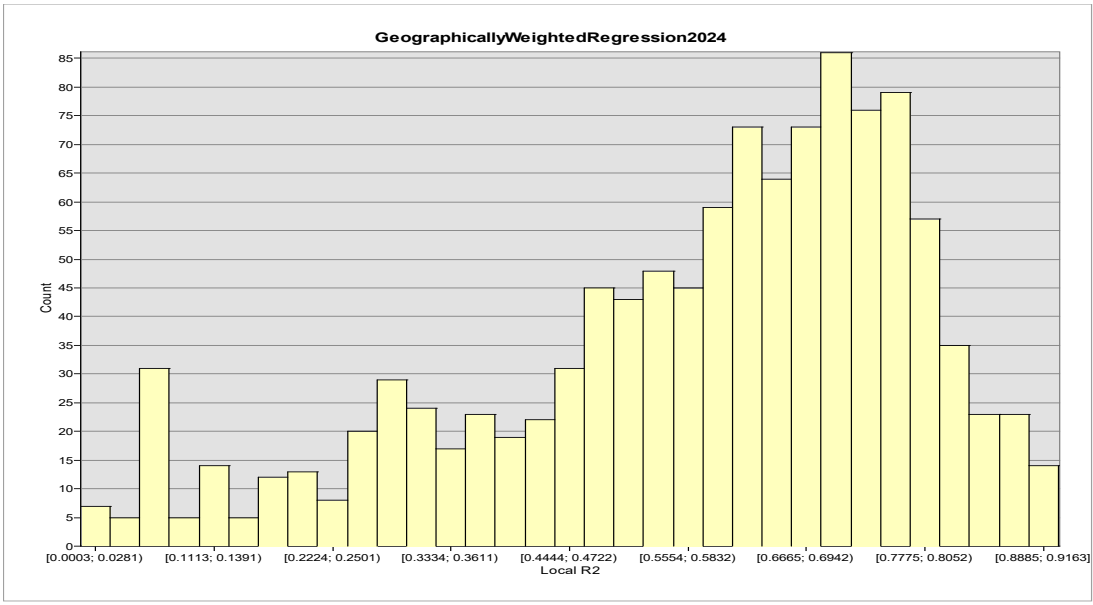

Figure 11. Histogram of local R^2 values for the geographically weighted regression (GWR) model in analyzing the relationship between land surface temperature (LST) and environmental indices for the year 2024

In Figure 12, the local R^2 values across various regions of Rasht city are represented with different colors. The darker shades represent higher local R^2 values, while lighter shades correspond to lower values. The red and orange areas indicate high local R^2 values, which signify more accurate LST predictions in these regions. These areas generally exhibit good model performance and show a strong correlation between LST and environmental indices. In contrast, the blue and green areas on the map represent lower local R^2 values. These areas, typically found in regions with significant land use changes or unique environmental characteristics, highlight zones where the model's prediction accuracy is lower.

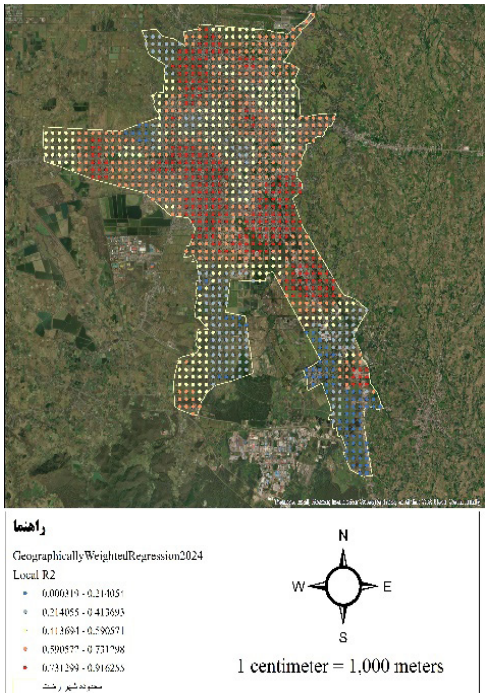

Figure 12. Local R^2 for the geographically weighted regression (GWR) model in analyzing the relationship between land surface temperature (LST) and environmental indices for the year 2024

Statistical description of LST variables for the year 2000

This section provides the statistical description of the land surface temperature (LST) variable for the year 2000. The analysis includes the calculation of key statistical values for the LST data in this specific period. The following values are computed to assess the spatial and temporal variations of LST in Rasht city:

- Mean LST: represents the average temperature across the study area.
- Min LST: the lowest observed LST value.
- Max LST: the highest observed LST value.
- Standard deviation: reflects the variability of temperature across different regions in the city.

These statistics help in understanding the distribution and fluctuations of temperature over time and will aid in evaluating the accuracy of regression models, particularly the geographically weighted regression (GWR) model, for predicting LST across different regions of Rasht city.

Table 8. Statistical description of the land surface temperature (LST) variable for the year 2000

Index	Value
Observed LST - mean	31.59°c
Observed LST - min	23.77°c
Observed LST - max	39.27°c
Predicted LST - mean	31.62°c
Predicted LST - min	23.76°c
Predicted LST - max	38.35°c
Residual - mean	-0.03°c
Residual - max	+4.30°c
Residual - min	-3.66°c

Comparison of observed (real LST) and predicted (predicted LST) land surface temperature (LST) using the GWR model

In Figure 13, the relationship between the observed land surface temperature (LST) and the predicted LST, as calculated by the geographically weighted regression (GWR) model, is examined for the given time period. The vertical axis of this plot displays the observed LST values, derived from actual observations. In contrast, the horizontal axis represents the predicted LST values generated by the GWR model for the same regions. Upon evaluating this chart, it can be observed that most of the data points are scattered around the diagonal line, indicating an acceptable agreement between the predicted and observed values. The closer the data points are to this line, the higher the model's accuracy in predicting the temperature. This good alignment in most regions reflects the model's correct performance in predicting land surface temperature. However, some data points are deviating from the diagonal line, indicating greater residuals and discrepancies between the predictions and actual observations. These points are typically found in areas with unique geographic or environmental characteristics, where the model may have struggled to simulate them accurately.

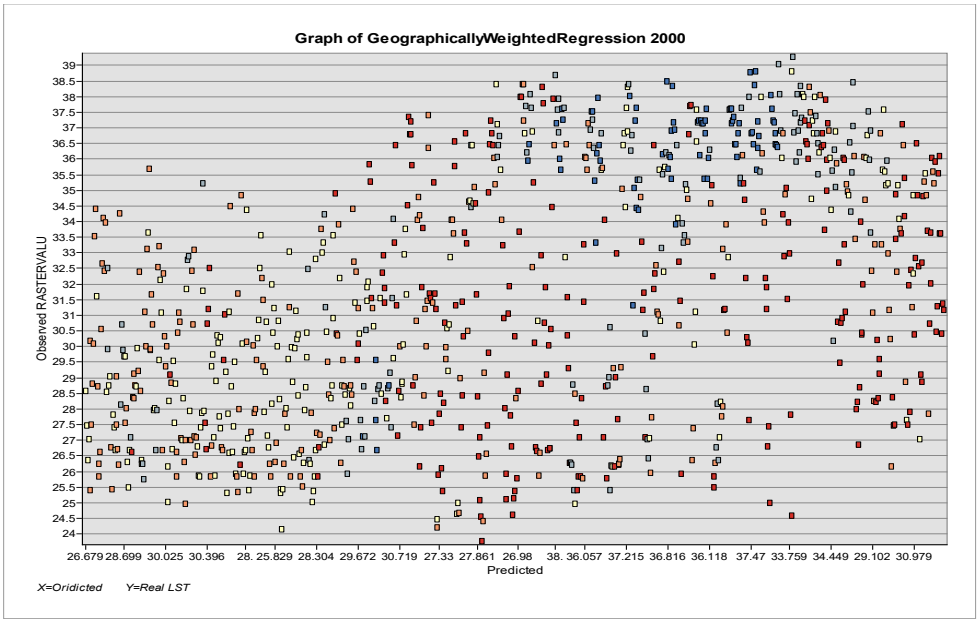

Figure 13. Scatter plot comparing real LST and predicted LST from the GWR model

Boxplot of residuals from the geographically weighted regression (GWR) model for the year 2000

In Figure 14, the residuals (errors) of the geographically weighted regression (GWR) model for the year 2000 are shown, clearly depicting the distribution and scatter of the residuals. The median of the residuals, which is close to zero, indicates the relative accuracy of the model's predictions. This means that the GWR model has generally provided accurate predictions, with minimal differences between the predicted and observed values. However, there are some outliers around the boxplot, which lie outside the natural range of the data. These points represent large residuals, indicating areas where the model struggled to make accurate predictions. The presence of these outliers suggests that in certain geographic regions or specific conditions, the model may have lower accuracy. Overall, the higher concentration of residuals around the median in the boxplot indicates the model's good performance; however, the outliers warrant further attention and analysis to identify the underlying causes of the discrepancies.

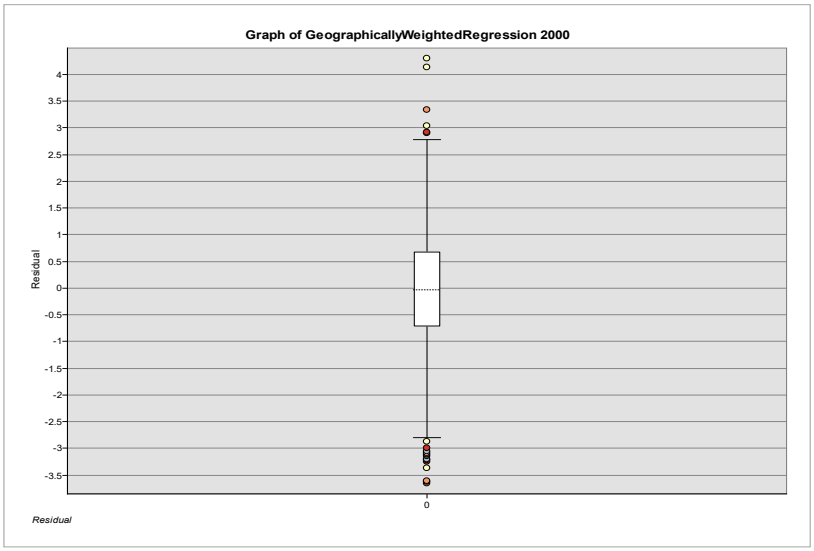

Figure 14. Boxplot of residuals from the geographically weighted regression (GWR) model

Evaluation of the quality of the geographically weighted regression (GWR) model for analyzing the relationship between LST and environmental indices in the year 2000

This section focuses on evaluating the performance of the geographically weighted regression (GWR) model in analyzing the relationship between land surface temperature (LST) and environmental indices. The model's quality is assessed using the local R^2 coefficient, which indicates the degree to which the model fits the data at the regional level. The table provided (Table 9) presents the local R^2 values for the year 2000, showing the mean, minimum, and maximum values. The mean local R^2 value of 0.68 indicates good model performance in predicting LST variations across the overall region. The minimum local R^2 value of 0.13 suggests low model accuracy in specific areas, which may require further improvements. On the other hand, the maximum local R^2 value of 0.92 indicates high accuracy and a good model fit in certain areas, suggesting that the model successfully captures LST changes in these regions. These results provide insights into both the strengths and limitations of the GWR model in different areas of Rasht city. Areas with higher local R^2 values indicate where the model has performed well. In comparison, areas with lower local R^2 values highlight regions that may require further refinement or additional factors to achieve improved prediction accuracy.

Table 9. Distribution of local R^2 values for the geographically weighted regression (GWR) model in analyzing the relationship between land surface temperature (LST) and environmental indices for the year 2000

Statistic	Value
Mean local R^2	0.68
Minimum local R^2	0.13
Maximum local R^2	0.92
Interquartile range (IQR)	0.13 - 0.92

This histogram shows the distribution of local R^2 values in the GWR model for the year 2000. Local R^2 represents the degree of model fit at the regional level, and this plot helps us visualize the spread and distribution of these values across the data. Most of the local R^2 values fall between 0.60 and 0.90, indicating good model performance in the majority of areas. However, the lower local R^2 values on the left side of the graph suggest that, in some regions, the model's predictions were not very accurate, indicating the need for model improvement in those specific areas.

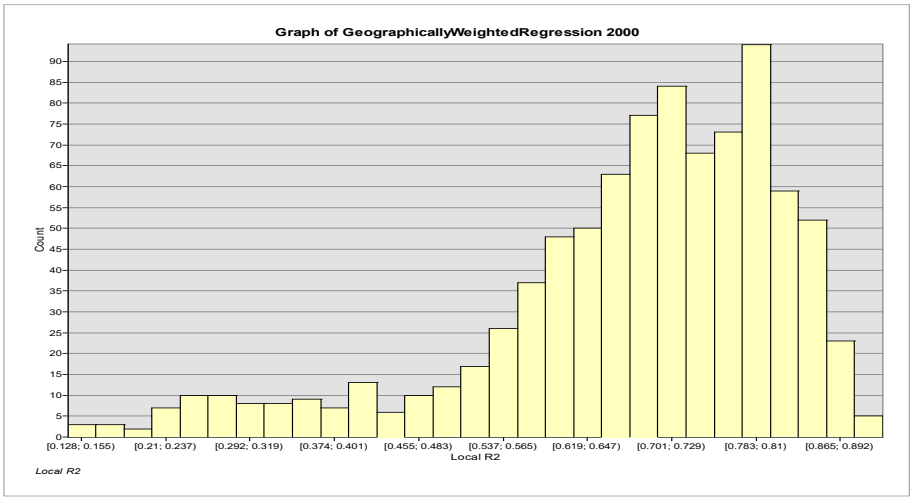

Figure 15. Histogram of local R^2 distribution for the geographically weighted regression (GWR) model in analyzing the relationship between land surface temperature (LST) and environmental indices for the year 2000

The map provided in Figure 16 shows the local R^2 values for the geographically weighted regression (GWR) model in the year 2000, illustrating the relationship between land surface temperature (LST) and geographic features at various locations. The map examines explicitly the connection between LST and geographic characteristics through the GWR model, with local R^2 values represented in color. In the map, red areas represent regions with high local R^2 values, indicating that the GWR model has made highly accurate predictions in these regions. These areas are typically found in central locations and some regions close to urban areas, suggesting that the model was more accurate in predicting LST in these zones. This accuracy could be attributed to the model's ability to simulate similar geographic characteristics or common environmental factors effectively. On the other hand, blue areas, which represent low local R^2 values, indicate that the model struggled to provide accurate predictions in these regions. These areas are typically located on the periphery or in more remote regions, away from urban centers, where the model's prediction accuracy is lower. This issue could stem from unique geographic features or insufficient data in these areas, which the model could not simulate effectively. The yellow and orange areas represent medium local R^2 values, indicating that the model's predictions were reasonably accurate, albeit with some discrepancies in these regions. These areas represent regions where the model performed better than in other areas, but still requires improvement in certain sections.

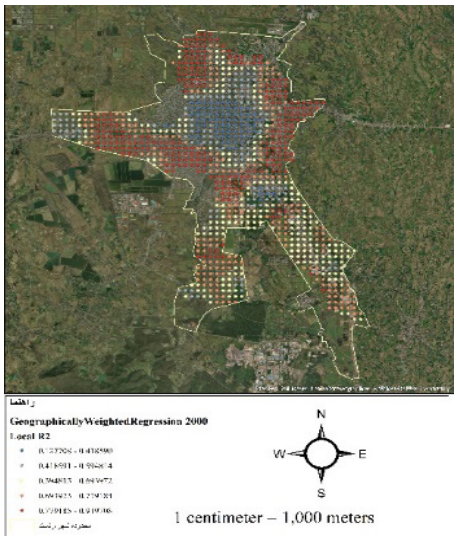

Figure 16. Local R^2 for the geographically weighted regression (GWR) model in analyzing the relationship between land surface temperature (LST) and environmental indices for the year 2000

Temporal trends and the relationship between land surface temperature (LST) and key indices from 2000 to 2024

Understanding the temporal dynamics between land surface temperature (LST) and biophysical-urban indices provides crucial insights into the drivers of the urban heat island (UHI) phenomenon and its ecological consequences. In this study, four key indices, including the normalized difference vegetation index (NDVI), normalized difference built-up index (NDBI), enhanced built-up and bare soil index (EBBI), and dry built-up index (DBI), were analyzed concurrently with LST data for four time periods (2000, 2008, 2016, and 2024). These indices represent complementary aspects of land cover structure:

- NDVI indicates vegetation greenness and potential for evapotranspiration.
- NDBI differentiates impermeable surfaces and built-up areas.
- EBBI increases the ability to distinguish between bare soils and urban areas by combining thermal information.
- DBI improves the identification of built-up areas in dry and semi-dry regions by reducing spectral errors between dry soils and urban surfaces.

The simultaneous analysis of these indices with LST changes aimed at three objectives:

1. Identifying temporal patterns of changes in LST and selected indices.
2. Investigating correlations and interactions between vegetation, imperviousness, and thermal responses.
3. Explaining the spatial-temporal processes influencing the intensification or moderation of the UHI phenomenon in Rasht during the study period.

Additionally, figures, tables, and accompanying descriptions display the analytical and comparative relationship between each index and LST.

Relationship between NDVI and LST

The temporal correlation between vegetation cover (NDVI) and land surface temperature (LST), as shown in Figure 17, indicates a consistent negative relationship throughout the study period. This means that an increase in vegetation cover (and consequently in evapotranspiration) leads to a decrease in LST, helping mitigate the UHI effect. In 2000, the correlation coefficient of approximately -0.75 reflected a strong inverse relationship, with dense vegetation in the southern and western regions associated with lower LST values. In contrast, the urban core and eastern parts had lower NDVI and higher surface temperatures. In 2008, the correlation strengthened (-0.80), indicating a relative recovery of vegetation, the establishment of local cooling effects, and the implementation of conservation policies during that period. In 2016, the relationship weakened (-0.65) due to rapid urban expansion, replacement of green areas with impermeable surfaces, and an increasing temperature contrast between the city center and the periphery. By 2024, the correlation coefficient slightly recovered (-0.78), aligning with the implementation of urban green projects (such as the eastern forest parks) and the use of reflective building materials (high albedo). Overall, the decrease in NDVI in the central and northern parts of the city is identified as a key factor in increasing LST and intensifying UHI. Urban green policies and the protection of natural belts have enhanced the negative NDVI-LST relationship and increased the thermal resilience of Rasht. Additionally, graphs, tables, and detailed descriptions in the following sections provide further analysis of the relationship between this index and LST.

Table 10. Relationship between NDVI and LST in Rasht (2000–2024)

Year	Mean NDVI	Mean LST (°c)	Correlation coefficient (NDVI–LST)	Interpretation
2000	~0.25	~35	≈ −0.75	Strong inverse relationship; limited urban development.
2008	~0.30	~33	≈ −0.80	Improved vegetation cover; slight reduction in temperature.
2016	~0.20	~37	≈ −0.65	Unsustainable development; increased thermal disparity.
2024	~0.35	~34	≈ −0.78	Relative improvement linked to green policies.

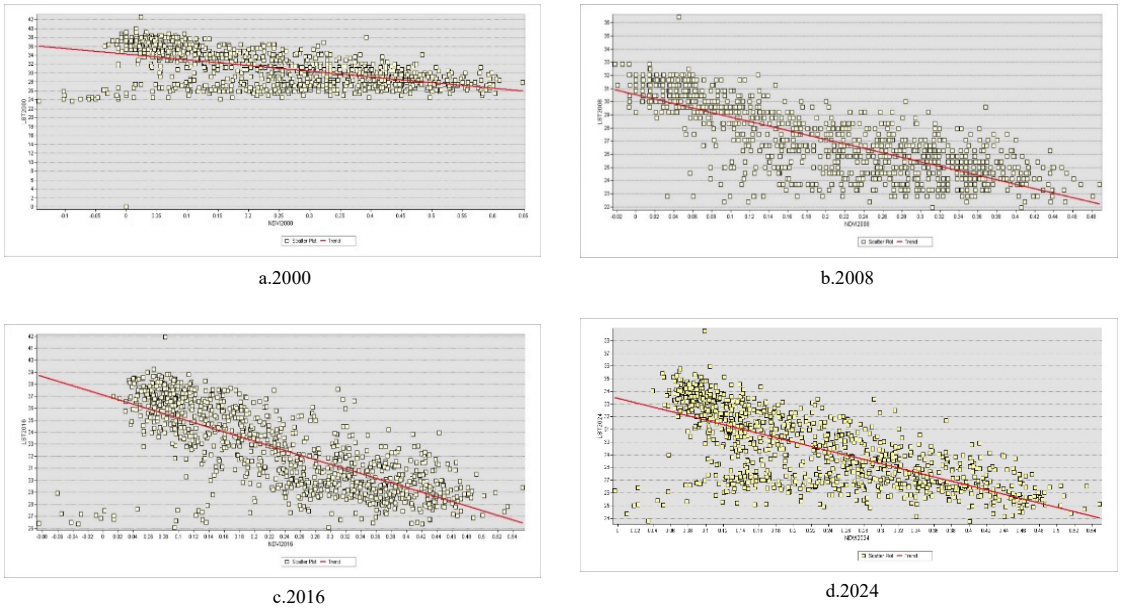

a.2000 b.2008

c.2016 d.2024

Figure 17. Regression relationships between the NDVI and land surface temperature (LST) in Rasht for the years 2000, 2008, 2016, and 2024 (from left to right).

The relationship between NDBI and LST

As depicted in Figure 18, the NDBI–LST relationship is positive in all years and strengthens from 2000 to 2024; as impervious/built surfaces increase, surface temperatures rise accordingly. The correlation increases from r ≈ 0.50–0.60 (2000) to 0.60–0.70 (2008), 0.70–0.75 (2016), and reaches approximately 0.80 (2024), indicating a steeper trend and tighter clustering around the fitted line. In 2000, despite a positive association, a wide scatter, and the presence of negative NDBI values (vegetated/wet areas), which correspond to lower LST in parts of the city, there was evidence of a cooling effect. In 2008, the slope steepens, and scatter decreases; negative-NDBI points decline while positive-NDBI points with higher LST become more frequent. In 2016, the LST range widens, and hot clusters at positive NDBI intensify, consistent with the expansion of contiguous urban land uses. By 2024, point concentrations in positive NDBI (0–0.12) and high LST (≈32–42 °c), together with the steep slope, show that the coupling between imperviousness and surface warming peaks, while the share of negative-NDBI areas diminishes.

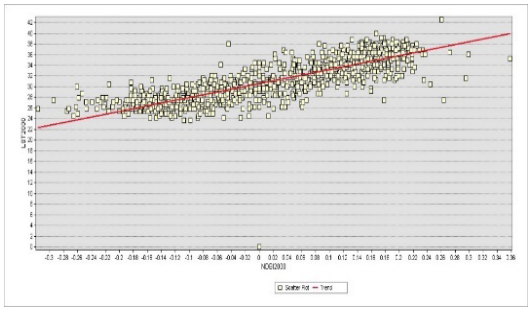

a.2000

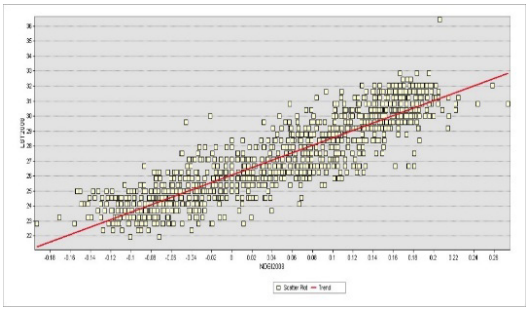

b.2008

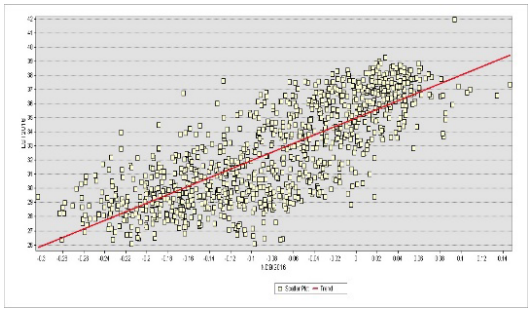

c.2016

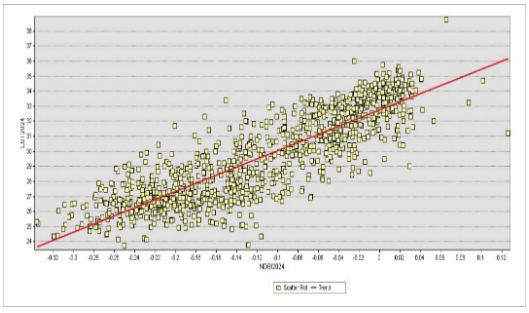

d.2024

Figure 18. Regression relationships between NDBI and LST in Rasht for the years 2000, 2008, 2016, and 2024 (from left to right).

The relationship between EBBI and LST

The four scatterplots demonstrate that the enhanced built-up and bareness index (EBBI), which integrates thermal information to better capture built-up and bare land surfaces, maintains a consistently positive and significant relationship with land surface temperature (LST) across all periods. In other words, as the extent of impervious and bare surfaces increases, LST also rises. By incorporating a thermal component, EBBI provides a more stable and physically coherent link with surface heat storage and release compared to purely spectral indices. In 2000, the fitted slope is positive but relatively mild. The wide scatter and the presence of low EBBI values highlight vegetated and moist zones associated with lower LST, where the cooling effect of peripheral landscapes remains pronounced. By 2008, the slope becomes steeper, and data points cluster more tightly around the regression line, with fewer low-EBBI values and a greater share of medium-to-high EBBI linked to elevated LST consistent with urban expansion and the reduction of green or moist patches. In 2016, the relationship strengthened further, and the LST range broadened, with hot clusters at higher EBBI values reflecting the role of industrial/commercial surfaces, as well as more continuous built fabric, in intensifying surface heating. Meanwhile, low EBBI areas persisted but with a reduced influence. By 2024, the slope remains high, and dispersion is more controlled. The concentration of points within mid-to-high EBBI, coupled with high LST, illustrates that the link between bare/built surfaces and surface warming has reached full maturity. However, a limited number of low-EBBI points continue to reveal the cooling contribution of green and moist belts in the southern and western sectors.

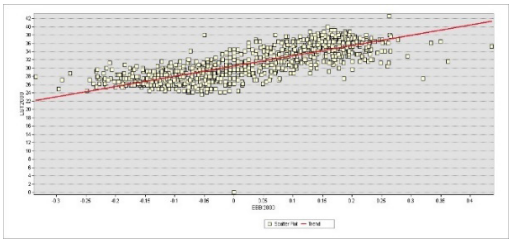

a.2000

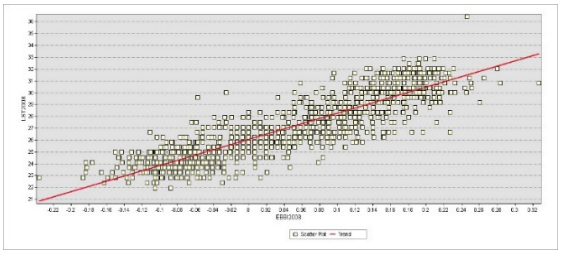

b.2008

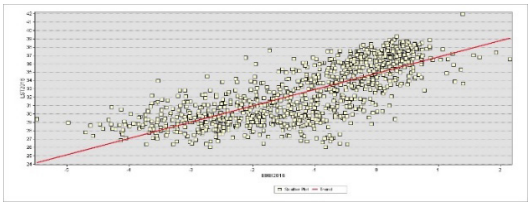

c.2016

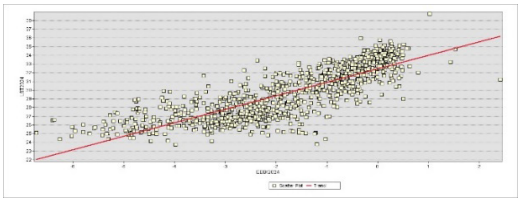

d.2024

Figure 19. Regression relationships between the enhanced built-up and bareness index (EBBI) and land surface temperature (LST) in Rasht for the years 2000, 2008, 2016, and 2024 (from left to right).

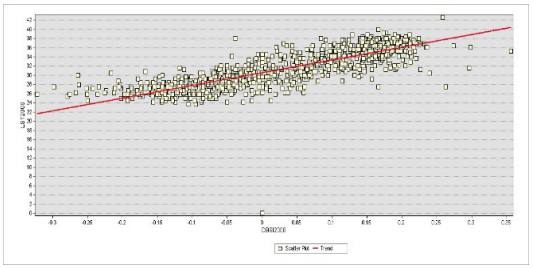

a.2000

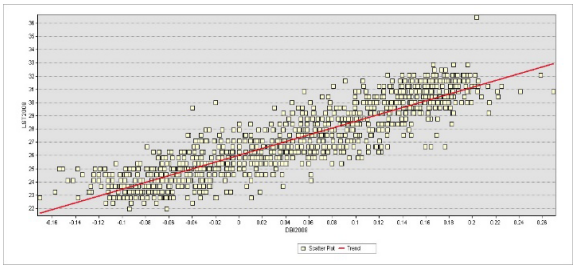

b.2008

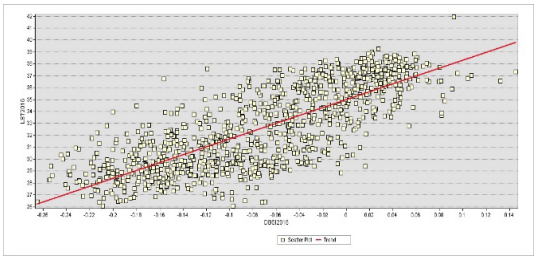

c.2016

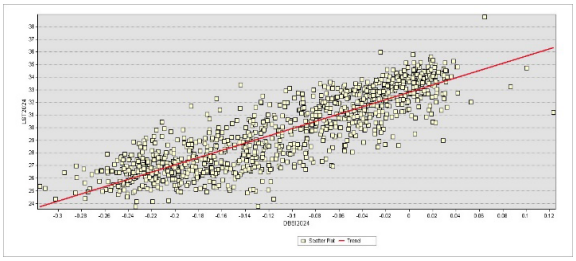

d.2024

Figure 20. Regression relationships between the dry built-up index (DBI) and land surface temperature (LST) in Rasht for 2000, 2008, 2016, and 2024 (left to right)

The results indicate that a measurable and statistically significant relationship exists between land use/ vegetation cover and land surface temperature (LST) in Rasht. Between 2000 and 2024, the urban class increases from 41% (~4,128 ha) to ~63% (~6,368 ha), while agricultural/orchard lands decline from 46% to ~21%; natural vegetation falls from 9.4% in 2000 to 2.7% in 2008, rises to 16.7% in 2016, and reaches 15.2% in 2024, whereas barren land (3.8% in 2000) is virtually eliminated. These shifts occur mainly in the south and east and are aligned with losses of green–moist cooling covers (rice paddies, orchards, natural vegetation, and wetland/moist-soil tracts). The NDVI–LST correlation remains negative and significant in all years (≈−0.72 in 2000, ≈−0.85 in 2008, ≈−0.60 in 2016, and ≈−0.78 in 2024), and NDVI ranges corroborate this pattern; localized decreases in the southwest coincide with higher temperatures, whereas relative gains in the east are accompanied by attenuated heat. In contrast, built-surface indices exhibit a positive and significant association with LST and remain stable throughout the study period. The EBBI differentiates

very hot urban patches from cooler agricultural areas and quantifies the more moderate behavior of mixed-use zones. Notably, the DBI (approximately ranging from −2 to +2) exhibits the most substantial alignment with LST and UHI intensity. In the multivariate model, the pattern of low NDVI with high NDBI and high DBI maps precisely corresponds to the most intense heat hotspots. The UHI index defined as the difference between each pixel's temperature and the rural background mean shows intensification from 2000 to 2016 and partial moderation by 2024: the maximum increases from ~2.23 (2000) to ~2.67 (2016) and then declines to ~2.47 (2024); the mean rises from 0.55 (2000) to 0.71 (2016) and ~0.72 (2024). The 2024 maps indicate a land-use-consistent structure: the city center (~+1.8 to +2.3) and the north (~+1.2 to +1.8) are the warmest sectors; the east is more moderate (~+0.8 to +1.5); and the south (~−0.5 to +0.33) and west (~−0.6 to +0.2) record the lowest intensities.

4. Discussion

The findings of this study indicate that the increase in the urban area share, from approximately 41% to about 63%, coupled with a reduction in agricultural and orchard areas from around 46% to about 21% between 2000 and 2024, has significantly transformed the surface heating pattern in Rasht city. The peak intensity of heating was observed in 2016, followed by a relative decrease in 2024. However, the background temperature across the city did not exhibit a significant change at the macro scale, with most fluctuations occurring in the thermal peaks and the relative intensity of the surface urban heat island (SUHI). Throughout the study period, the relationship between NDVI and LST remained negative and statistically significant, though the strength of this correlation fluctuated over time. The correlation coefficient increased from approximately -0.75 in 2000 to -0.80 in 2008, weakened to around -0.65 in 2016, and slightly recovered to -0.78 in 2024. This pattern aligns with changes observed in NDVI and LULC maps. In 2008, the distribution of vegetation and green-agricultural belts in the periphery was more continuous and widespread compared to 2000. However, by 2016, there was greater fragmentation in green patches within and around the city. In 2024, although the overall vegetation cover was lower than in 2000, some improvement in NDVI and the reappearance of denser green patches were observed in certain sub-catchments and peripheral belts, which corresponds with the relative strengthening of the negative NDVI–LST correlation. In this context, changes in the NDVI–LST correlation are interpreted solely in relation to the amount and spatial configuration of vegetation cover, as well as the city's expansion pattern. No direct attribution is made to specific interventions or policies, as such data were not available for this study.

Spatially, the thermal pattern across the four time periods remained relatively stable: the central core and northeastern axis remained the hottest areas, while the green–moist belts in the south and west were the coolest. Spectral indices reinforce this interpretation: a) NDBI and EBBI exhibit a positive correlation with LST, indicating that areas with a dominant combination of built surfaces and bare soils, particularly in mixed-use regions, tend to fall into higher or medium-temperature classes. Given the presence of thermal components in the EBBI definition, the correlation between this index and LST is interpreted as a spectral-spatial alignment, rather than an independent causal relationship; b) On the other hand, DBI exhibits the highest ability to differentiate thermal clusters, and its combination with low NDVI values precisely overlaps with the areas with the highest thermal intensity. In multivariate models, the co-occurrence of low NDVI with high NDBI and DBI efficiently delineates hotspots, indicating that the reduction in green cover and the increase in the continuity of impervious surfaces are the primary drivers of SUHI intensification at the intra-urban scale. The operational definition of urban heat island (UHI) in this study, as the temperature difference of each pixel relative to the surrounding background, indicates that the intensity of the phenomenon gradually increased from 2000 to 2016 and moderated in 2024. This pattern suggests that the increase in continuity and expansion of built surfaces (particularly in the central core and eastern-northeastern corridors) and the weakening of green networks during the earlier period intensified the SUHI effect. The relative reduction in intensity in the later period is more related to the decrease in maximum temperatures and the shift in the spatial distribution of hot spots than to changes in the overall thermal baseline of the city. from the perspective of land-use diversity and vegetation structure, the evidence suggests that wherever green–moist cover continuity and adequacy were preserved or restored, SUHI intensity decreased, and the temperature contrast between the urban core and its surroundings weakened. This finding is consistent with

global studies on the cooling role of green and blue infrastructure (Esposito et al., 2024; Yang et al., 2017) and shows that agricultural–wetland belts in the south and west of Rasht play a crucial role in mitigating thermal peaks. Compared to cities in different climates and scales, the observed pattern in Rasht is explainable: in Wuhan, continuous expansion of impervious surfaces and linear development along transportation corridors was associated with increased SUHI; a similar pattern of a ring–axial structure has also emerged in Rasht since 2016 (Tian et al., 2025). In Tehran, a reduction in vegetation and high urban density reinforced central thermal peaks, increasing the spatial dependence of SUHI on activity centers, similar to the thermal concentration observed in the core of Rasht (Zargari et al., 2024). In Semarang, long-term urbanization trends have intensified SUHI and confirmed the cooling role of surrounding green belts, similar to the performance of agricultural–wetland belts in the south and west of Rasht (Sejati et al., 2019). Bucharest's findings also show that land-use change and urban morphology determine the intensity and extent of SUHI, similar to Rasht's transition from a monocentric to a more circular and relatively polycentric structure (Sejati et al., 2019). Overall, these patterns suggest that the reduction in evapotranspiration, the high thermal storage capacity of surfaces, and the persistence of low-albedo surfaces are common physical mechanisms for surface heating. However, Rasht's humid and lowland conditions accentuate the thermal contrast between the urban fabric and the surrounding green, moist areas.

The causal explanation of findings in this study is based on three main mechanisms:

1. Vegetation reduces thermal load: the stable negative NDVI–LST relationship across the period aligns with evapotranspiration processes and shading effects, reflecting the "green-blue park effect" in various climates (Yang et al., 2017).

2. Continuity of built surfaces, especially in dense cores and traffic corridors, increases heat storage and sensible heat fluxes. This relationship has been confirmed in morphological analyses and empirical evidence from other cities.

3. Composite indices that simultaneously consider spectral dryness and thermal signals, such as DBI and EBBI, perform better than purely reflective indices in identifying thermal patches in humid environments. However, when interpreting the correlation between these indices and LST, attention must be paid to the shared thermal component, as their primary role is to spatially differentiate impervious surfaces and bare soils.

As a result, the dynamics of SUHI in Rasht show an increasing trend until 2016, followed by a relative decrease in 2024. This change can be explained by the increased continuity of built-up areas and the weakening of green networks during the first period, as well as the combination of LULC changes with climatic fluctuations in the recent period. However, the results indicate that these changes have not yet been sufficient to change the overall thermal baseline of the city, and the thermal background of the city still remains dominated by the expansion of impervious surfaces (Esposito et al., 2024; Sobrino & Irakulis, 2020). From both scientific and practical perspectives, this study offers three main contributions to the urban heat island literature in humid lowland cities:

1. A data-driven RS–GIS framework has been applied to Rasht, integrating indices like NDVI, NDBI, EBBI, and DBI alongside LULC maps and LST data over the long period of 2000 to 2024. While this methodology relies on established techniques, it fills a research gap regarding SUHI dynamics in such environments at a local scale.

2. The study documents the persistent thermal hot spots in the central core and eastern–northeastern axes, as well as the substantial spatial overlap between impervious surface continuity, reduced NDVI, and increased SUHI. These relationships have been elucidated through statistical correlations and spatial co-occurrence, offering coherent evidence of the link between compact urban growth and the intensification of surface heating.

3. Based on the spatial–temporal patterns, a set of policy recommendations for managing SUHI in Rasht has been derived, including the need for the protection of southern and western agricultural–wetland belts, strengthening continuous urban green corridors, and improving albedo and permeability in dense urban fabrics. These suggestions are formulated as local adaptations of globally recognized thermal adaptation principles, tailored to Rasht's specific climatic and morphological context (Esposito et al., 2024).

This spatio-temporal narrative addresses the existing research gap on humid lowland cities in Iran. It indicates that preserving surrounding cooling belts in these cities may have a more substantial thermal moderating effect compared to arid cities, a key consideration for local policy-making in Rasht. Furthermore, similar studies on multi-hazard resilience assessments in planning, such as those by Sarker et al.

(2023), can align heat mitigation actions with multi-hazard resilience strategies in Rasht, thereby contributing to the development of adaptive and more resilient urban policies.

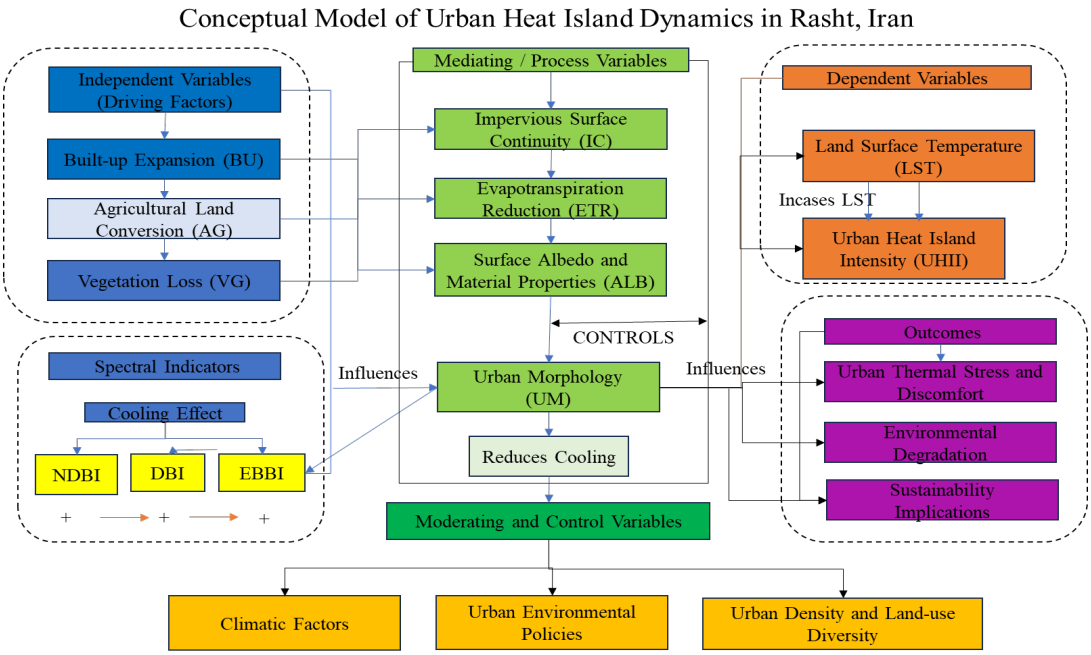

Figure 21. Conceptual model of urban heat island (UHI) dynamics in the city of Rasht

5. Conclusion

The findings of this study indicate that the expansion and connectivity of impermeable surfaces in the city of Rasht, particularly in the central core and along the east-northeast/southeast–east corridor, have coincided with the intensification of the surface urban heat island (SUHI). Meanwhile, the gradual fragmentation of the urban green corridors and surrounding agricultural belts has weakened their cooling capacity. Results from geographic weighted regression (GWR) models in spatial analyses indicate that environmental indices, such as NDVI and NDBI, have a significant impact on LST. A reduction in NDVI in urban areas is associated with an increase in LST and the intensification of the urban heat island effect. In contrast, an increase in NDBI and DBI contributes to higher surface temperatures in urban areas. These changes clearly highlight the impact of urban development on surface heating. Throughout the four time periods examined (2000, 2008, 2016, and 2024), the average and range of LST fluctuated. After a temporary decrease in 2008, it peaked in 2016 and showed a relative adjustment in 2024. However, the central thermal cores and the principal development axes remained stable throughout the years, with the SUHI spatial pattern showing more changes in intensity and extent rather than location. During the study period, the NDVI–LST relationship remained negative and statistically significant in all years, while the indices NDBI, DBI, and, to some extent, EBBI exhibited a positive correlation with surface temperatures. This pattern suggests that the reduction in greenery and the increased connectivity of built-up surfaces are associated with higher LST and intensified SUHI. However, these relationships are interpreted as spatial correlations rather than causal links.

Morphologically, the thermal structure of Rasht has evolved from a dense monocentric pattern to one with a warm middle ring and signs of emerging multicentricity, consistent with the compression of urban form and the radial expansion of built-up areas. In areas with more balanced land use and sufficient green–moist coverage, SUHI intensity is significantly lower, and the temperature contrast between the city center and its periphery is diminished. These findings align with global literature on the cooling role of green and blue infrastructures and the heat-amplifying effects of impermeable surfaces (Esposito et al., 2024; yang et al., 2017; tian et al., 2025), while also showing that in a humid, lowland city like Rasht, the southern and western agricultural–wetland belts act as thermal buffers and their preservation is essential for moderating the thermal contrast between the urban core and the green–moist periphery.

Based on these findings, the policy implications of this research can be summarized in three main points: a) the protection and reconnection of green–agricultural belts and their integration with urban green patches to strengthen the continuous green–moist network; b) targeted interventions in the central core and the east-northeast/southeast–east corridors through the increase of tree canopy shade in street spaces, development of linear parks, green rooftops, facades, and the use of high-albedo and permeable materials in pavements and building shells to reduce heat storage during the day and nighttime warming; c) the establishment of a periodic monitoring system for NDVI, NDBI, and LST in critical areas to assess the comparative impact of policies and continuously update urban planning tools. In addition to these morphological interventions, the evidence from heat-vulnerable cities emphasizes the necessity of integrating social considerations; in Rasht, low-income groups and informal workers face the highest exposure to extreme heat in areas with high LST. Therefore, early warning systems for heat, inclusive housing designs, and access to public cooling spaces should be considered in conjunction with spatial interventions to ensure equitable thermal resilience.

Methodologically and practically, this study makes three main contributions to the SUHI literature in humid lowland cities. First, a data-driven RS–GIS framework has been applied to Rasht, integrating indices such as NDVI, NDBI, EBBI, and DBI alongside LULC and LST maps from 2000 to 2024. This approach, although based on established methods, fills the spatial–climatic gap regarding SUHI dynamics in lowland humid cities in Iran at a local scale. Second, a consistent pattern of thermal hotspots focusing on the urban core and eastern city axes, with substantial spatial overlap in connectivity with impermeable surfaces and decreasing NDVI, has been documented. This pattern provides consistent evidence of the link between the expansion of compact urban forms and the intensification of surface heating, which can serve as a basis for more detailed causal analyses in future studies—third, based on these spatial–temporal patterns, a set of policy recommendations for managing SUHI in Rasht has been provided, aligning well-established heat reduction principles (such as protecting green belts, increasing albedo, and improving surface permeability) with the specific morphological and climatic conditions of the city.

At the same time, this study faces two main limitations: first, reliance on summer satellite images, which limits the generalization of results to annual and seasonal scales due to cloud coverage in other seasons; second, reliance on spectral indices and surface temperature, which do not replace field measurements of temperature, humidity, and thermal properties of materials. Overall, the results of this study show that reconfiguring spatial patterns by reducing the connectivity of impermeable surfaces and reconstructing a continuous green–moist network, along with integrating social and multi-risk considerations in urban policymaking, provides a realistic pathway for reducing peak surface temperatures, moderating the thermal baseline, and enhancing sustainable thermal resilience in Rasht. Future research should include field validation using temperature and humidity sensor networks, analysis of vegetation cover composition and structure, soil moisture, and the radiative–thermal properties of materials in densely populated areas, as well as the application of spatio-temporal machine learning models for predicting urban growth and evaluating policy scenarios. Additionally, utilizing multi-risk assessment frameworks, such as fuzzy–AHP models, can align SUHI reduction with simultaneous risk management (floods, runoff, and land-use changes) and contribute to the development of adaptive urban policies.

Authors' Contributions

The first and second authors have contributed equally to the writing of this article.

Acknowledgments

This article is derived from the Master's thesis titled "Investigating the Impact of Land Use Diversity and Vegetation Cover Structure on the Intensity of Urban Heat Islands in the Urban Area of Rasht," written by Shahryar Rezaei in the Department of Urban Planning, Faculty of Architecture and Arts, University of Guilan, under the supervision of Dr. Ali Akbar Salari Poor. This article does not have any material or moral sponsors.

Conflict of Interest

The authors declare that they have no conflict of interest.

References

Alhazmi, Mansour, David J. Sailor, Jyothis Anand (2022). A new perspective for understanding actual anthropogenic heat emissions from buildings. *Energy and Buildings*, Volume 258, 111860. https://doi.org/10.1016/j.enbuild.2022.111860

Benayad, Mohamed, Mohamed Rabii Simou, Abdelilah Rochd, Nouriddine Houran, Mehdi Maanan, Hassan Rhinane (2025). Using Deep Learning to create an Enhanced Basemap from

RGB Satellite Images for Urban Planning. *Natural Hazards Research*, ISSN 2666-5921. https://doi.org/10.1016/j.nhres.2025.09.006

Esposito, A., Pappaccogli, G., Donateo, A., Salizzoni, P., Maffeis, G., Semeraro, T., ... & Buccolieri, R. (2024). Urban morphology and surface urban heat island relationship during heat waves: A study of Milan and Lecce (Italy). *Remote Sensing*, 16(23), 4496. https://doi.org/10.3390/rs16234496

Feng, Rundong, Fuyuan Wang, Kaiyong Wang, Hongjie Wang, Li Li (2021). Urban ecological land and natural-anthropogenic environment interactively drive surface urban heat island: An urban agglomeration-level study in China. *Environment International*, Volume 157, 106857. https://doi.org/10.1016/j.envint.2021.106857

Gazi, M.Y., Rahman, M.Z., Uddin, M.M. et al. (2021). Spatio-temporal dynamic land cover changes and their impacts on the urban thermal environment in the Chittagong metropolitan area, Bangladesh. *GeoJournal*, 86, 2119–2134. https://doi.org/10.1007/s10708-020-10178-6

Jang, Seonju, Jinhyun Bae, YouJoung Kim (2024). Street-level urban heat island mitigation: Assessing the cooling effect of green infrastructure using urban IoT sensor big data. *Sustainable Cities and Society*, Volume 100, 105007. https://doi.org/10.1016/j.scs.2023.105007

Karimi, Bashir Ahmad, Mohammad Aslam Haziq, Athiqullah Hayat (2025). Specific impacts of climate change on the hydrological patterns and land use dynamics in the Arghandab River Basin, Kandahar, Afghanistan. *Natural Hazards Research*, Volume 5, Issue 2, Pages 380-390. https://doi.org/10.1016/j.nhres.2024.12.007

Koko, A. F., Yue, W., Abubakar, G. A., Alabsi, A. A. N., & Hamed, R. (2021). Spatiotemporal Influence of Land Use/Land Cover Change Dynamics on Surface Urban Heat Island: A Case Study of Abuja Metropolis, Nigeria. *ISPRS International Journal of Geo-Information*, 10(5), 272. https://doi.org/10.3390/ijgi10050272

Li, Xiaoma, Yuyu Zhou, Sha Yu, Gensuo Jia, Huidong Li, Wenliang Li (2019). Urban heat island impacts on building energy consumption: A review of approaches and findings. *Energy*, Volume 174, Pages 407-419. https://doi.org/10.1016/j.energy.2019.02.183

P. Rao, P., Tassinari, P., & Torreggiani, D. (2023). Exploring the land-use urban heat island nexus under climate change conditions using a machine learning approach: A spatio-temporal analysis of remotely sensed data. *Heliyon*, 9(8). https://doi.org/10.1016/j.heliyon.2023.e18423

Ramsay, Emma E., Grant A. Duffy, Kerrie Burge, Ruzka R. Taruc, Genie M. Fleming, Peter A. Faber, Steven L. Chown (2023). Spatio-temporal development of the urban heat island in a socioeconomically diverse tropical city. *Environmental Pollution*, Volume 316, Part 1, 120443. https://doi.org/10.1016/j.envpol.2022.120443

Rundong Feng, Fuyuan Wang, Kaiyong Wang, Hongjie Wang, Li Li (2021). Urban ecological land and natural-anthropogenic environment interactively drive surface urban heat island: An urban agglomeration-level study in China. *Environment International*, Volume 157, 106857. https://doi.org/10.1016/j.envint.2021.106857

Sarker, Sajib, Mohammed Sarfaraz Gani Adnan (2024). Evaluating multi-hazard risk associated with tropical cyclones using the fuzzy analytic hierarchy process model. *Natural Hazards Research*, Volume 4, Issue 1, Pages 97-109. https://doi.org/10.1016/j.nhres.2023.11.007

Sejati, Anang Wahyu, Imam Buchori, Iwan Rudiarto (2019). The spatio-temporal trends of urban growth and surface urban heat islands over two decades in the Semarang Metropolitan Region. *Sustainable Cities and Society*, Volume 46, 101432. https://doi.org/10.1016/j.scs.2019.101432

Shahfahad, Talukdar, S., Rihan, M. et al. (2022). Modelling urban heat island (UHI) and thermal field variation and their relationship with land use indices over Delhi and Mumbai metro cities. *Environ Dev Sustain*, 24, 3762–3790. https://doi.org/10.1007/s10668-021-01587-7

Sharma, A., Vashishtha, D. (2023). Spatio-temporal Assessment of Land Use Land Cover Changes and Their Impact on Variations of Land Surface Temperature in Aligarh Municipality. *J. Indian Soc. Remote Sens*., 51, 799–827. https://doi.org/10.1007/s12524-022-01652-2

Sharmin, Tania, Adrian Chappell (2025). Detecting the changing impact of urbanization on urban heat islands in a tropical megacity using local climate zones. *Energy and Built Environment*, ISSN 2666-1233. https://doi.org/10.1016/j.enbenv.2025.02.002

Sheikh Mohiuddin Shahrujjaman, Bivuti Bhushan Sikder, Dilara Zahid, Bikash Pal (2025). Heat wave adaptation strategies among informal workers in an urban setting: A study in Dhaka City, Bangladesh. *Natural Hazards Research*, Volume 5, Issue 3, Pages 509-522. https://doi.org/10.1016/j.nhres.2025.01.006

Siswanto, Siswanto, Danang Eko Nuryanto, Muhammad Rezza Ferdiansyah, Ova Candra Dewi, Ahmad Gamal, Muhammad Dimyati (2023). Spatio-temporal characteristics of the urban heat Island of Jakarta metropolitan. *Remote Sensing Applications: Society and Environment*, Volume 32, 101062. https://doi.org/10.1016/j.rsase.2023.101062

Sobrino, J. A., & Irakulis, I. (2020). A methodology for comparing the surface urban heat island in selected urban agglomerations around the world from Sentinel-3 SLSTR data. *Remote Sensing*, 12(12), 2052. https://doi.org/10.3390/rs12122052

Tanoori, Ghazaleh, Ali Soltani, Atoosa Modiri (2024). Machine Learning for Urban Heat Island (UHI) Analysis: Predicting Land Surface Temperature (LST) in Urban Environments. *Urban Climate*, Volume 55, 101962. https://doi.org/10.1016/j.uclim.2024.101962

Tan, J.K.N., R.N. Belcher, H.T.W. Tan, S. Menz, T. Schroepfer (2021). The urban heat island mitigation potential of vegetation depends on the local surface type and the amount of shade it receives. *Urban Forestry & Urban Greening*, Volume 62, 127128. https://doi.org/10.1016/j.ufug.2021.127128

Tang, J., Di, L., Xiao, J., Lu, D., & Zhou, Y. (2017). Impacts of Land Use and Socioeconomic Patterns on Urban Heat Islands. *International Journal of Remote Sensing*, 38(11), 3445–3465. https://doi.org/10.1080/01431161.2017.1295485

Tian, J., Chen, Y., Yang, L., Li, D., Liu, L., Li, J., & Tang, X. (2025). Enhancing Urban Flood Susceptibility Assessment by Capturing the Features of the Urban Environment. *Remote Sensing*, 17(8), 1347. https://doi.org/10.3390/rs17081347

Wang, Aijia, Chen Ren, Junqi Wang, Zhuangbo Feng, Prashant Kumar, Fariborz Haghighat, Shi-Jie Cao (2024). Health assess-

ment and mitigation solutions to heat pollution induced by urban traffic. *Journal of Cleaner Production*, Volume 434, 140097. https://doi.org/10.1016/j.jclepro.2023.140097

Wang, C., Myint, S. W., Wang, Z., & Song, J. (2016). Spatio-Temporal Modeling of the Urban Heat Island in the Phoenix Metropolitan Area: Land Use Change Implications. *Remote Sensing*, 8(3), 185. https://doi.org/10.3390/rs8030185

Wei, Yufei, Rémi Lemoy, Geoffrey Caruso (2024). The effect of population size on urban heat island and NO2 air pollution: Review and meta-analysis. *City and Environment Interactions*, Volume 24, 100161. https://doi.org/10.1016/j.cacint.2024.100161

Xiang, Xiaoyang, Zhihong Zhai, Chengliang Fan, Yunfei Ding, Lifei Ye, Jiangbo Li (2024). Modelling future land use and land cover changes and their impacts on urban heat island intensity in Guangzhou, China. *Journal of Environmental Management*, Volume 366, 121787. https://doi.org/10.1016/j.jenvman.2024.121787

Yang, C., He, X., Yan, F., Yu, L., Bu, K., Yang, J., Chang, L., & Zhang, S. (2017). Mapping the Influence of Land Use/Land Cover Changes on the Urban Heat Island Effect—A Case Study of Changchun, China. *Sustainability*, 9(2), 312. https://doi.org/10.3390/su9020312

Yao, Y., Chang, C., Ndayisaba, F., & Wang, S. (2020). A new approach for surface urban heat island monitoring based on a machine learning algorithm and a spatiotemporal fusion model. *IEEE Access*, 8, 164268-164281. [doi: 10.1109/ACCESS.2020.3022047]

Zafar, Z., Zha, Y., Fahd, S. et al. (2024). The interplay between urbanization, vegetation loss, and surface heat islands in cities: Two decadal empirical evidences from Pakistan. *Theor. Appl. Climatol.*, 155, 9911–9928. https://doi.org/10.1007/s00704-024-05214-z

Zargari, M., Mofidi, A., Entezari, A. et al. (2024). Climatic comparison of surface urban heat island using satellite remote sensing in Tehran and its suburbs. *Sci Rep*, 14, 643. https://doi.org/10.1038/s41598-023-50757-2